DEPARTMENT OF AEROSPACE ENGINEERING
COLLEGE OF ENGINEERING AND TECHNOLOGY
OLD DOMINION UNIVERSITY
NORFOLK, VA 23529

SUBSONIC AND SUPERSONIC JET NOISE CALCULATIONS USING PSE AND DNS

By
Dr. P. Balakumar, Principal Investigator
Farouk Owis
Department of Aerospace Engineering

FINAL TECHNICAL REPORT

For the period ending September 30, 1998

Prepared for
NASA Langley Research Center
Attn.: Ms. Barbara S. Thomson
Grants Officer
Mail Stop 126
Hampton, VA 23681-2199

Dr. Michele Macaraeg, Technical Officer

Under
Research Grant NAG-1-2054
ODURF File No. 182431

March 1999

Jet stability and Noise Prediction Using Parabolized Stability Equations

Prediction of Supersonic Jet Noise

P. Balakumar
Aerospace Engineering Department,
Old Dominion University, Norfolk, Virginia 23529–0247

Abstract

Noise radiated from a supersonic jet is computed using the Parabolized Stability Equations (PSE) method. The evolution of the instability waves inside the jet is computed using the PSE method and the noise radiated to the far field from these waves is calculated by solving the wave equation using the Fourier transform method. We performed the computations for a cold supersonic jet of Mach number 2.1 which is excited by disturbances with Strouhal numbers St=.2 and .4 and the azimuthal wavenumber m=1. Good agreement in the sound pressure level are observed between the computed and the measured (Troutt and McLaughlin 1980) results.

1. Introduction

In this work we computed the noise radiated from supersonic turbulent jets using the PSE (Parabolized Stability Equations) method. Jet noise can be divided into three categories: (1) shock-induced screech tone noise; (2) shock-induced broad band noise; and (3) turbulent mixing noise. The screech tone appears in an imperfectly expanded jet as discrete band in the front part of the jet. The screech tone phenomena is very complex and it is believed that the toroidal and helical vortices which shed at the lip of the nozzle interact with the shocks when they propagate downstream and makes the shock to oscillate and this radiates sound in the upstream direction at discrete frequency. In an imperfectly expanded jet, the shock-cells formed by the oblique shocks or the expansion fans generated at nozzle lip interact with the large scale turbulence and generate broad band noise. The dominant part of the broad band shock-associated noise is comprised of a spectral peak with a relatively narrow half-width. Turbulent mixing noise is the noise component which is contributed from the large-scale and small scale turbulence in the jet. For a perfectly expanded supersonic jet, the noise is completely generated by the turbulence in the jet and the predominant part of the noise is radiated in the downstream direction in the range between 25–45°. It is observed that at low Reynolds numbers the noise is radiated at a discrete frequency which is closer to the most unstable instability wave for that jet. At moderate and high Reynolds numbers there is discernible peak but they become broad band. These similarities between the noise generated from the high and low Reynolds number jets imply that the noise generation mechanisms in supersonic jets are same at different Reynolds numbers. Several experiments were performed to identify these mechanisms (McLaughlin et al. 1975, 1977, Morrision and McLaughlin 1979, 1980, Troutt and McLaughlin 1982, Seiner et al. 1993) and it is concluded that the dominant part of the turbulent mixing noise of high Reynolds number supersonic jets is generated by the large-scale coherent structures. It is also concluded

that these large-scale coherent structures are the instability waves of the jet (Tam 1971, 1972, Morris and Tam 1977, Tam et. al. 1991).

The jet column can be divided into three regions, namely, laminar, transitional and turbulent. The extent of the laminar and transitional region depends on the Reynolds number and the Mach number. The laminar region extends a few diameters from the exit and the disturbances grow exponentially in this region. Further downstream, when the amplitude of these disturbances becomes large, they interact nonlinearly and then saturate. These instability waves then disengage their coherence and disintegrate, and the flow becomes turbulent. In a series of detailed experiments (McLaughlin et al. 1975, Morrison and McLaughlin 1979, 1980, Troutt and McLaughlin 1982), it was confirmed that most of the noise is generated in this region where the disturbances saturate and decay. It is also identified that this region is always close to the end of the potential core region.

Several methods are explored in practice to compute the turbulent mixing noise generated from supersonic jets. One is the multiple scale approach (Tam 1991). In this method it is assumed that the flow field induced by the large scale structures in a turbulent jet can be modelled as the flow field generated by the evolution of instability waves in a given turbulent flow. The mean flow is obtained from the experimental measurements or by solving the Reynolds averaged Navier-Stokes equations. The local growth rate, the wavenumber and the eigenfunctions of a disturbance with a constant frequency and a fixed azimuthal wavenumber are obtained by solving the compressible Rayleigh's stability equations and the nonparallel corrections are determined using the multiple scale and the adjoint method. After computing the flow field in the near field of the jet, the acoustic field in the outer part of the jet is calculated by solving the wave equation. In the second method, the mean flow field and the flow field associated with the large scale structures are computed by solving the Large-Eddy-Simulation equations with the subgrid scale modelling (Mankbadi et. al. 1994). The noise in the far field is again obtained by solving the linearized Euler equations. In the third method, the complete Navier-Stokes equations are solved (Mitchell et. al. 1996) to obtain the inner and the outer acoustic fields. The last two methods are more accurate and do not make any assumptions other than the subgrid scale modelling in the LES approach. However, they are computationally very expensive compared to the first method.

In this work we followed the first approach and compute the flow field in the inner part of the jet using the PSE method instead of using the multiple scale method and compute the acoustic field in the outer region by solving the wave equation with the pressure obtained from the PSE as the inner boundary data. We obtained the mean flow by curve fitting the experimental data by cubic splines.

2. Formulation

We are concerned with the evolution of a small disturbance of a single frequency and a fixed azimuthal wavenumber inside an axisymmetric supersonic jet and the noise radiated from this disturbance field to the outer part of the jet. Figure 1 shows the schematic and the coordinate system that we used in the analysis. We perform the computation in two steps. In the first step, we compute the flow field inside the jet using the PSE method and in the second step we solve

the wave equation to compute the acoustic field in the far field of the jet. Since we are seeking linear solutions, the disturbance quantities can be written in the form

$$q(x,r,\theta,t) = \tilde{q}(x,r)e^{im\theta - i\omega t}, \tag{1}$$

where x, r and θ are the axial, radial and the azimuthal coordinates; m is the mode number in the azimuthal direction, ω is the frequency and t is the time; q is a vector,

$$q = \{u,v,w,p,T\}^T, \tag{2}$$

and u, v and w are velocity components in the x, r, and θ directions, p is the pressure and T is the temperature. We non-dimensionalize the variables as follows:

velocity ~ U_j : jet exit velocity
Temperature ~ T_0 : ambient temperature
Density ~ ρ_0 : ambient density.
Mach number based on the jet exit conditions ~ $M_j = \frac{U_j}{\sqrt{\gamma RT_j}}$.
Mach number based on the jet exit velocity and the free stream temperature ~ $M_0 = \frac{U_j}{\sqrt{\gamma RT_0}}$.

2.1 The Parabolized Stability Equations

In the parabolized stability equations (PSE) approach, one attempts to construct an approximate solution of the full Navier-Stokes equations. The idea was first introduced by Herbert(1991) and applied to linear and non-linear Blasius boundary-layer flow by Bertolotti (1992). Now it has been developed and has been applied to two and three-dimensional incompressible and compressible boundary-layer flows and supersonic jets (Chang et.al. 1994 , Malik et.al 1994, Balakumar 1994, Malik et.al 1997). We give a brief description of PSE for a general flow and apply to jets as a special case.

In the linear parallel stability analysis, the disturbance quantities are written in normal mode form. If q(x,y,z,t) is a flow variable in normal mode analysis, we write

$$q(x,y,z,t) = \tilde{q}(y)e^{i\int \alpha dx + i\beta z - i\omega t} \tag{3}$$

Here ω is the frequency of the disturbance, β is the azimuthal or spanwise wave number, and α(x) is the wavenumber in the axial direction. The eigenfunction is $\tilde{q}$(y) which is function of y (normal coordinate) only. We substitute this expression into the linearized Navier-Stokes equations and, assuming the flow is parallel in the streamwise direction , we obtain an ordinary differential equation for $\tilde{q}$(y). This equation, along with the homogeneous boundary condition at the wall (for boundary-layer flow) and in the free-stream, forms the eigenvalue problem for the wave number α and for the eigenfunction $\tilde{q}$(y).

In practice, the mean flow is not constant, but varies in the streamwise direction. Since this variation is relatively slow, the wavenumber α and the eigenfunction $\tilde{q}$(y) vary slowly in the streamwise direction. In the PSE approach, we use this fact to construct an approximate solution to the Navier-Stokes equations. In the PSE formulations, we write the disturbance quantities as

$$q(x,y,z,t) = \tilde{q}(x,y)e^{i\int \alpha dx + i\beta z - i\omega t} \tag{4}$$

where $\tilde{q}$(x,y) represents the amplitude part and the exponent as the wave part.

The first and the second derivatives of q(x,y,z,t) are

$$\frac{\partial q}{\partial x} = \left\{ i\alpha(x)\tilde{q}(x,y) + \frac{\partial \tilde{q}}{\partial x} \right\} e^{i\int \alpha dx + i\beta z - i\omega t} \tag{5}$$

$$\frac{\partial^2 q}{\partial x^2} = \left\{ -\alpha^2(x)\tilde{q}(x,y) + i\frac{d\alpha}{dx}\tilde{q}(x,y) + 2i\alpha\frac{\partial \tilde{q}}{\partial x} + \frac{\partial^2 \tilde{q}}{\partial x^2} \right\} e^{i\int \alpha dx + i\beta z - i\omega t}. \tag{6}$$

Since the amplitude part q varies slowly in the x direction in the PSE approximation, we neglect $\frac{\partial^2 \tilde{q}}{\partial x^2}$ and write the second derivative as

$$\frac{\partial^2 q}{\partial x^2} = \left\{ -\alpha^2(x)\tilde{q}(x,y) + i\frac{d\alpha}{dx}\tilde{q}(x,y) + 2i\alpha\frac{\partial \tilde{q}}{\partial x} \right\} e^{i\int \alpha dx + i\beta z - i\omega t}. \tag{7}$$

Therefore, if we substitute this approximation into the Navier-Stokes equations, the second derivative in the x direction drops out and the system of equations is parabolized. The solution may be found by marching in the x-direction which is the major advantage of PSE.

The first step of the procedure is to start, as in any other parabolic problem, with a known solution at $x=x_0$, $\tilde{q}(x=x_0,y)$, $\alpha(x=x_0)$, assume $\alpha(x=x_0+\Delta x)=\alpha(x=x_0)$, march the PSE equation to the next station $x=x_0+\Delta x$, and solve for $\tilde{q}(x=x_0+\Delta x,y)$. The second step is to compute the new $\alpha(x=x_0+\Delta x)$ from the computed $\tilde{q}(x=x_0+\Delta x,y)$. The problem is that since $\tilde{q}$ is a function of y, and $\tilde{q}$ can be any physical quantity (e.g., velocity, temperature, mass flow rate, etc.), it is not clear how to compute α. This problem arises in the experiments too. If we want to measure growth rate using hot wires, we face the same problem as to which quantity and at what location we want to measure. Therefore in a nonparallel flow, there is no unique wavenumber as in the parallel linear theory. We call the wave number we compute the "wave number based on some quantity (e.g., velocity, temperature, mass-flow rate)". Usually the wave number is computed at the location in the shear layer where the flow quantities become maximum. For example, if

we choose to compute the wave number α at the location where streamwise velocity u peaks, α is obtained from the relation

$$\alpha(x = x_0 + \Delta x) = \frac{1}{iu_{max}} \left(\frac{\partial u}{\partial x} \right)_{y=\bar{y}} \tag{8}$$

where $\bar{y}$ is the location where u peaks and i=$\sqrt{-1}$. In the third step after the newα(x=x_0+Δx) at x=x_0+Δx is determined, the marching computations are repeated at this location with the newα(x=x_0+Δx). This procedure is continued until the change in α is less than some prescribed value ($\sim 10^{-10}$). After the convergence is obtained at this station, we march to the next station. This basically explains the PSE method. Next we briefly describe the governing equations and the numerical procedure that we used to solve the PSE equations.

Let x_1, x_2, x_3 be a set of generalized orthogonal curvilinear coordinates and the metric coefficients are h_1, h_2, h_3 and the velocities in the direction 1, 2, 3 are u_1, u_2, u_3. The mean flow quantities are represented by $Q^0 = \{U_1, U_2, U_3, T, p, \rho\}^T$ and the disturbance quantities are represented by $Q' = \{u_1', u_2', u_3', \theta', p', \tau'\}^T$. Therefore, the total variables are

$$Q = Q^0 + Q' \tag{9}$$

Substituting this in the governing equations and substracting the mean-flow terms, we obtain the equations for Q'. As discussed earlier, Q' is split into the amplitude and wave part

$$Q' = \tilde{Q}(x_1, x_3) e^{i \int \alpha dx_1 + i\beta x_2 - i\omega t}. \tag{10}$$

Substituting this expression into the governing equations for Q' and neglecting the nonlinear terms we obtain the following linear PSE equations for $\tilde{Q}$,

$$\begin{aligned} A\frac{\partial^2 \tilde{Q}}{\partial x_3^2} + B\frac{\partial \tilde{Q}}{\partial x_3} + C\tilde{Q} = \\ D\frac{\partial \tilde{Q}}{\partial x_1} + E\frac{\partial^2 \tilde{Q}}{\partial x_1 \partial x_3}. \end{aligned} \tag{11}$$

Here, A, B, C, D and E are (5×6) matrices which are functions of Q^0 and its derivatives, ω, α, β and the metrices h_1, h_2, h_3. These equations are solved by first discretizing the x_1 derivative by two point upwind scheme and second by applying the fourth order central difference scheme in the normal direction. When we apply this to an axi-symmetric jet, the variables and the metrics becomes x_1=x, x_2=θ, x_3=r, h_1=1, h_2=r, h_3=1 and β=m. The velocities in the axial, azimuthal and in the radial directions are u, w and v.

Since the governing equations are singular at r=0, the appropriate boundary conditions and the governing equations have to be derived separately. We use L'Hospital's rule at r=0 and obtain

the appropriate governing equations and the boundary conditions. The boundary conditions at r=0 takes different form based on the azimuthal mode number m. They take the following form:

$\underline{m = 0}$

$$\frac{\partial u}{\partial r} = 0, \quad v = 0, \quad w = 0, \quad \frac{\partial \theta}{\partial r} = 0. \tag{12}$$

$\underline{m = \pm 1}$

$$u = 0, \quad w + i\frac{|m|}{m}v = 0, \quad \theta = 0. \tag{13}$$

$\underline{m \geq 2}$

$$u = 0, \quad v = 0, \quad w = 0, \quad \theta = 0. \tag{14}$$

In the far field $r \to \infty$, we use the condition

$$u = 0, \quad v = 0, \quad w = 0, \quad \theta = 0. \tag{15}$$

In the computations, we impose these boundary conditions at $r=50d_j$, where d_j is the diameter of the jet.

2.2 Wave Equation

To compute the acoustic field in the far field, we solve the linearized Euler equations using the Fourier Transform technique. In cylindrical coordinates the linearized Euler equations for the amplitude part $\tilde{q}(x, r)$ become

$$\begin{aligned}
-i\omega\tilde{v} &= -\frac{1}{\overline{\rho}}\frac{\partial \tilde{p}}{\partial r}, \\
-i\omega\tilde{w} &= -\frac{im}{\overline{\rho} r}\tilde{p}, \\
-i\omega\tilde{u} &= -\frac{1}{\overline{\rho}}\frac{\partial \tilde{p}}{\partial x}, \\
-i\omega\tilde{p} &+ \frac{1}{M^2}\left(\frac{\tilde{v}}{r} + \frac{\partial \tilde{v}}{\partial r} + \frac{im}{r}\tilde{w} + \frac{\partial \tilde{u}}{\partial r}\right) = 0.
\end{aligned} \tag{16}$$

Eliminating the velocity components , we obtain the wave equation for the pressure

$$\frac{\partial^2 \tilde{p}}{\partial r^2} + \frac{\partial^2 \tilde{p}}{\partial x^2} + \frac{1}{r}\frac{\partial \tilde{p}}{\partial r} + \left(\overline{\rho} M^2 \omega^2 - \frac{m^2}{r^2}\right)\tilde{p} = 0. \tag{17}$$

The boundary conditions are

$$\begin{aligned} &\tilde{p} \to 0, \text{ as } r \to \infty, \\ &\tilde{p}(x, r_0) = \tilde{p}_0(x), \text{ at } r = r_0. \end{aligned} \tag{18}$$

Here r_0 is the height at which the lower boundary for the wave equation is located and this line is in the region where the mean velocity becomes almost zero (Figure 1). Usually, we take r_0~ 2–3 diameters of the jet. $\tilde{p}_0(x)$ is the pressure distribution along the line r=r_0 which is known from the PSE calculations. The wave equation (eq. 13) is solved using the Fourier transform technique and the solution is given by

$$\begin{aligned} &\tilde{p}(x, r) = \int_{-\infty}^{\infty} \tilde{p}_0(k_x) \frac{K_m(r\lambda)}{K_m(r_0\lambda)} e^{ik_x x} dk_x, \\ &\lambda^2 = k_x^2 - \overline{\rho} M^2 \omega^2, \quad (Real(\lambda) > 0). \end{aligned} \tag{19}$$

Here K_m is the modified Bessel function of second kind of order m and the integration is along the contour C, which does not cross any branch cuts in the complex k_x – plane and is shown in Figure 2. We evaluated this integral numerically. For comparison and to determine analytically the intense noise radiation direction and the dominant wavenumber region, it is advantageous to evaluate this integral asymptotically for large distances. As it was done by Tam and Burton (1984), we rewrite this expression in spherical coordinates (R, X, ϕ). In the new coordinate system, the pressure expression becomes

$$\tilde{p}(x, r) = \int_{-\infty}^{\infty} \frac{\tilde{p}_0(k_x)}{K_m(r_0\lambda)} K_m(R sin X \lambda) e^{ik_x cos X R} dk_x. \tag{20}$$

For large R, the Bessel function and the integral become

$$\begin{aligned} &K_m(R sin X \lambda) = \left(\frac{\pi}{2R sin X \lambda}\right)^{\frac{1}{2}} e^{-R sin X \lambda}, \\ &\tilde{p}(x, r) = \sqrt{\frac{\pi}{2R sin X}} \int_{-\infty}^{\infty} \frac{\tilde{p}_0(k_x)}{K_m(r_0\lambda)} \frac{1}{\sqrt{\lambda}} e^{i(k_x cos X + i sin X \lambda)R} dk_x. \end{aligned} \tag{21}$$

This integral can be evaluated using the stationary phase method and the integration yields

$$\begin{aligned} &p(R, X, \phi, t) = \frac{2}{R} \left\{ \frac{\tilde{p}_0(M\omega cos X)}{K_m(r_0 M\omega sin X)} \right\} \\ &e^{i\left\{M\omega R + m\phi - \omega t - \frac{1}{2}(m+1)\pi\right\}}, \end{aligned} \tag{22}$$

and the stationary point is given by

$$k_x = M\omega cosX. \tag{23}$$

From this expression for a fixed R we can determine the maximum acoustic pressure and the direction of the maximum pressure and the wavenumber by evaluating the expression in the bracket in eq. (22)..

3. Results

Computations are performed for a cold supersonic jet of Mach number M_j=2.1. The mean flow velocity profiles are obtained by curve fitting the experimental data which is given in McLaughlin, Seiner & Liu (1980). We used the same empirical formulas as used by Tam & Burton (1982). The jet is divided into three regions as core, transitional and fully developed regions. In each region, different functions are used to represent the measured velocity profiles. The functions used are:

Core region : $0 < x < x_t$

$$\overline{U} = \left\{ \begin{array}{ll} 1 & (r < h), \\ exp\left[-(ln2)\left(\frac{r-h(x)}{b(x)}\right)^2\right] & (h \leq r). \end{array} \right\} \tag{24}$$

Transition region : $x_t < x < x_f$

$$\overline{U} = \left\{ \begin{array}{ll} u_c(x) & (r < h), \\ u_c(x)exp\left[-(ln2)\left(\frac{r-h(x)}{b(x)}\right)^2\right] & (h \leq r). \end{array} \right\} \tag{25}$$

Fully developed region : $x > x_f$

$$\overline{U} = \left\{ u_c(x)exp\left[-(ln2)\left(\frac{r}{b(x)}\right)^2\right] \right\}. \tag{26}$$

Here h(x) is the thickness of the core region, b(x) is the height from the end of the potential core to the half velocity point, $\bar{U}$=.5. x_t and x_f are the locations of the end of the core and the start of the fully developed regions from the nozzle exit. From the experimental results of McLaughlin, Seiner & Liu (1980), it is found that the core region extends up to five diameters and the fully developed region starts at eight diameters. b(x) is determined by approximating the measured thickness of the shear layer by a cubic spline curve. The variation of h(x) in the core region and the variation of u_c(x) in the fully developed region are obtained from the conservation of axial momentum condition. In the transition region, the variation of h(x) and u_c(x) are obtained by matching their absolute values and their derivatives at both ends. Figure 3 shows the measured and the curve fitted distribution of b(x) and figure 4 shows the corresponding variation of the centerline velocity u_c and the thickness of the core h(x) along the axis of the jet. The temperature

distribution is obtained by assuming that the total temperature is constant across the jet and the radial velocity is obtained by integrating the continuity equation in the radial direction.

After the mean flow profiles are obtained, the evolution of the disturbances inside the jet is computed using the PSE method. In all the previous computations, Euler equations are solved to obtain the flow field inside the jet. The main reason is that we are simulating a turbulent jet and it is difficult to define a Reynolds number in this case and further that the flow dynamics are of the inviscid type in free shear flows and the Reynolds number has little effect in the results. The PSE equations are derived from the complete viscous Navier-Stokes equations and we performed the computations as a viscous problem but fixing the Reynolds number arbitrarily at larger values ~ 10^6. We present the results for two Strouhal numbers St=.2 and .4 and for the helical mode m=1 which is the most amplified disturbance in an axisymmetric jet.

Figure 5 shows the evolution of the mass velocity fluctuations with the axial distance obtained from the nonparallel PSE calculations for the Strouhal numbers St=.2, .4 and m=1. The mass velocity fluctuations are measured at the radial location where they are maximum. Figures 6 and 7 show the real part and the amplitude of the pressure distribution in the axial direction at the radial location $\frac{r}{d_j} = 3$ for two Strouhal numbers St=.2 and .4. We observe that the pressure peaks at about $\frac{X}{d_j} = 8$ and decreases further downstream and we also notice that the wavelengths are smaller at St=.4 than that at St=.2.

Figures 8 and 9 show the spectral distribution of the pressure for the Strouhal numbers St=.2 and .4 obtained by taking the Fourier transform of the pressure distribution shown in the figures 6 and 7. The branch points in the complex k_x plane are located at $k_x = \pm\omega M$. For St=.2 and .4 these points are located at k_x=±1.922 and 3.844 respectively. The waves with the wavenumbers larger than these values travel subsonically relative to the free stream and hence will not radiate noise to the far field. Equation (22) shows that the far field noise is determined by the quantity $\frac{\tilde{p}_0(k_x)}{K_{m0}(k_x)}$ and the noise radiation direction and the wavenumber is related by the eq. (23). In figures 10 and 11 we plotted these two quantities for the Strouhal numbers St=.2 and .4 respectively. The figures show that the intense noise is radiated at an angle of 45° from the axis for the frequency St=.2 and the angle is 37° for St=.4. Figures 12 and 13 show the sound pressure levels (SPL in dB) radiated from the instability waves with the frequency St=.2, .4 and m=1 to the far field obtained by integrating the eq. (20) numerically. We see that the noise is radiated in a wedge shaped region and the intense noise is radiated in a fixed direction which is inclined at an angle of 44° for St=.2 and is inclined at 37° for St=.4 which agree with our earlier prediction from the asymptotic theory. Figures 14 and 15 show the experimental measurements of sound pressure levels by Trout and McLaughlin (1982) for a jet excited at St=.2 and .4. In figures 12 and 13 we matched the computed sound pressure levels with the experimental measurements shown in figures 14 and 15 at one point $\frac{X}{R_j} = 30$ and $\frac{r}{R_j} = 20$. It is seen that the agreement between the experiment and the computation is very good. In the experiment the noise is radiated at an angle of 44 and 36° which are exactly same as that predicted from the computations. To understand the character of the flow field inside the jet, in figure 16 we plotted the variation of the quantity

$$k_x\left(1 - \frac{c}{a_\infty}\right) \tag{27}$$

along the axis. Here c is the phase speed of the instability wave and a_∞ is the speed of sound in the freestream. If this quantity is positive the wave is travelling subsonically relative to the freestream and if it is negative it is travelling supersonically. We observe from the figure that the waves travel supersonically for the first 5 and 7 diameters for St=.2 and .4 respectively. After that they travel subsonically and further downstream they again travel supersonically. This figure depicts that the most of the noise is radiated from the first few diameters of the jet

4. Conclusions

In this work, the evolution of a small disturbance of a single frequency and a fixed azimuthal wavenumber inside an axisymmetric supersonic turbulent jet is computed using the PSE method and the noise radiated from this disturbance field to the outer part of the jet is evaluated by solving the wave equation using the Fourier transform method. The PSE computations are very efficient and take about 5 minutes on a SUN workstation. Computations are performed for a jet of Mach number 2.1 at two Strouhal numbers St=.2 and .4. Good agreements are found between the computed and the measured sound pressure levels. It is also observed that the waves travel supersonically for the first few diameters from the jet exit and after that they travel subsonically. This agrees with the observation that most of the noise in a supersonic jet is radiated from the first few diameters of the jet.

Acknowledgment

We wish to acknowledge the support from the NASA Langley Research Center under the grant NAG-1–1677.

References

1. Bertolotti, F. P., Herbert, Th. and Spalart, P. R., 1992 "Linear and Nonlinear Stability of the Blasius Boundary Layer," J. Fluid Mechanics, Vol. 242, pp. 441–474.

2. Balakumar, P. 1994 "Supersonic Jet Noise Prediction and Control," Contractor Report to NASA Lewis Research Center, Contract No. NAS3–27205.

3. Chang, C.-L., Malik, M. R.,199 "Oblique-mode breakdown and secondary instability in supersonic boundary layers," J. Fluid Mechanics, Vol 273, pp. 323–360.

4. Crow, S.C. and Champagne, F. H., 1971 "Orderly Structure in Jet Turbulence," J. Fluid Mechanics, Vol. 48, pt. 3, pp. 547–591

5. Herbert, Th., 1991 "Boundary-Layer Transition – Analysis and Prediction Revisited," AIAA Paper 91–0737.

6. Malik, M. R. and Chang, C. 1997 "PSE Applied to Supersonic Jet Instability," AIAA 97–0758, 35th Aerospace Sciences Meeting and Exhibit, Reno, NV, 1997.

7. Malik, M., Li, F. and Chang, C., 1994 "Crossflow disturbances in three-dimensional boundary layers; Nonlinear development, wave interaction and secondary instability," F. Fluid Mechanics, Vol. 316, pp. 1–36.

8. Mankbadi, R. R., Mayer, M.E., and Povinelli, L. 1994 "Structure of Supersonic Jet Flow and its Radiated Sound,"AIAA J. Vol. 32, No. 5.

9. McLaughlin, D. K., Morrison, G. L., and Troutt, T. R., 1977 " Reynolds Number Dependence in Supersonic Jet Noise," AIAA J., Vol. 15, pp. 526–532.

10. McLaughlin, D. K., Morrison, G. L., and Troutt, T. R., 1975 "Experiments on the Instability Waves in a Supersonic Jet and Their Acoustic radiation," J. Fluid Mechanics, Vol. 69, pp. 73–95.

11. McLaughlin, D. K., Seiner, J. M. and Liu, H., 1980 "On the noise generated by large scale instabilities in supersonic jets", AIAA Paper No. 80–0964.

12. Mitchell, B. E., Lele, S. K., and Moin, P. 1996 "Direct computation of the sound generated by subsonic and supersonic axisymmetric jets," Rep. TF-66. Thermoscience Divison, Department of Mechanical Engineering, Stanford University.

13. Morris, P. J., and Tam, C. K. W., 1977 "Near and far Field Noise for Large-Scale Instabilities of Axisymmetric Jets," AIAA Paper 77–1351.

14. Morrison, G. L. and McLaughlin, D. K., 1980 "Instability Process in Low Reynolds number Supersonic Jets," AIAA J., Vol. 18, No. 7, pp. 793–800.

15. Morrison, G. L. and McLaughlin, D. K., 1979 "The Noise Generated by Instabilities in Low Reynolds number Supersonic Jets," J. Sound and Vibration, Vol. 65, No. 2, pp. 171–191.

16. Seiner, J. M., Bhat, T. R. S., and Ponton, M. K., 1993 "Mach Wave Emission from a High Temperature Supersonic Jets," AIAA Paper 93–0734.

17. Tam, C. K. W., 1991 "Jet Noise Generated by Large-Scale Coherent Motion,' in Aeroacoustics of Flight Vehicles: Theory and Practise, Vol. 1: Noise Sources, NASA RP-1258, WRDC TR-90–3052.

18. Tam, C. K. W., 1972 "On the Noise of a Nearly Ideally Expanded Supersonic Jet," J. Fluid Mechanics, Vol. 51, pp. 69–95.

19. Tam, C. K. W., 1971 "Directional Acoustic Radiation from a Supersonic Jet Generated by Shear Layer Instability," J. Fluid Mechanics, Vol. 46, pp. 757–768.

20. Tam, C. K. W., and Burton, D. E., 1984 " Sound Generated by Instability Waves of Supersonic Flows. Part 2. Axisymmetric Jets, ," J. Fluid Mechanics, Vol. 138, pp. 273–295.

21. Tam, C. K. W., and Chen, P., and Seiner, J. M., 1991 " Relationship Between Instability Waves and Noise of High-Speed Jets," AIAA Paper 91–0492.

22. Troutt, T. R. and McLaughlin, D. K., 1982 "Experiments on the Flow and Acoustic Properties of a Moderate-Reynolds-Number Supersonic Jet," J. Fluid Mechanics, Vol. 116, pp. 123–156.

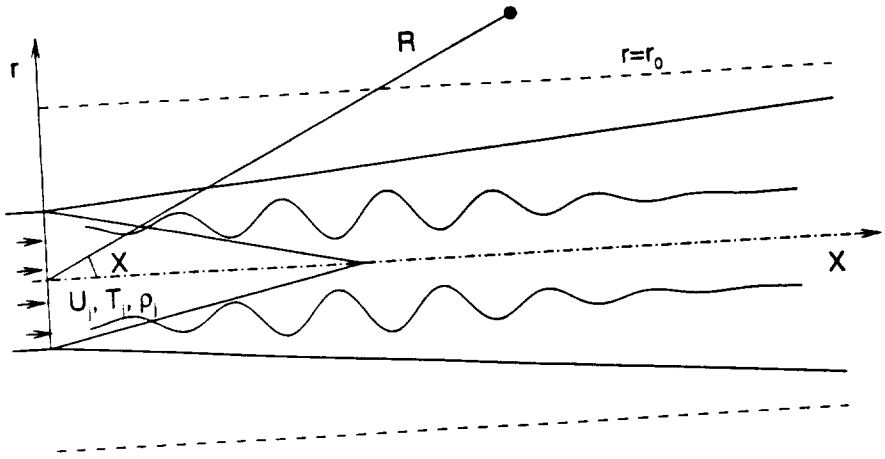

Figure 1. Schematic diagram of an axisymmetric jet.

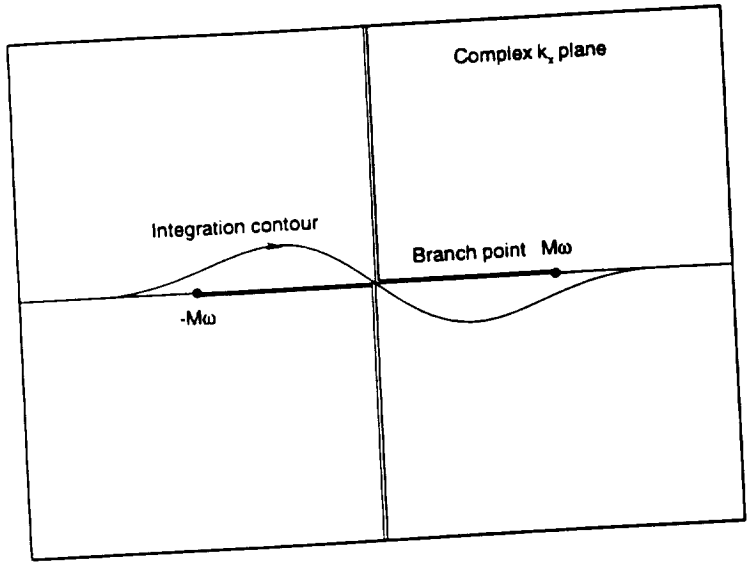

Figure 2. Integration contour in complex k_x plane.

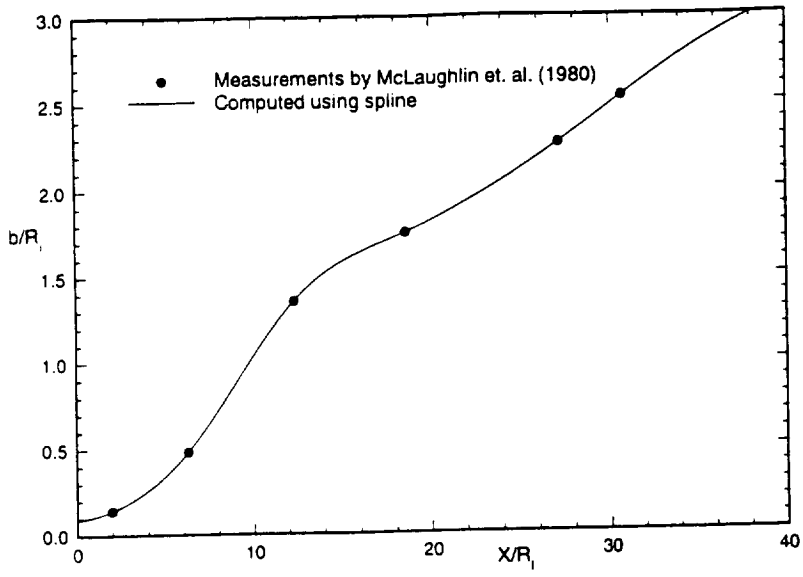

Figure 3. Axial distribution of mean velocity profile parameters b(x).

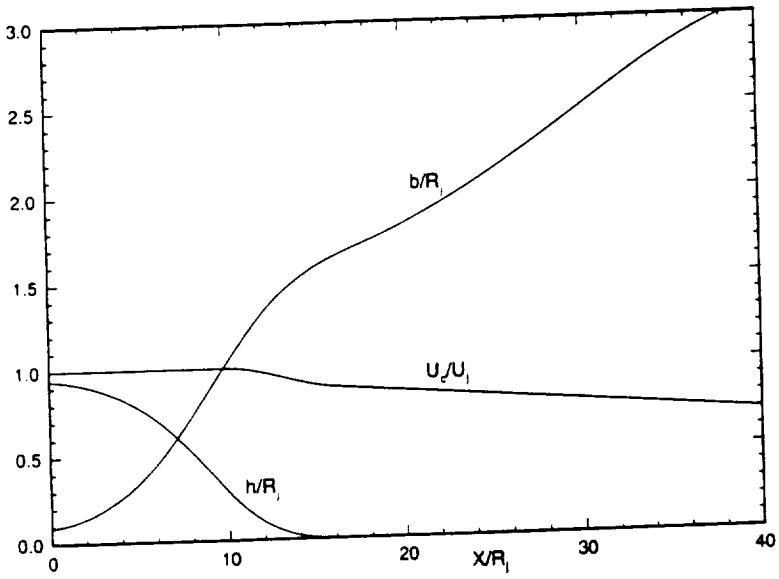

Figure 4. Axial distribution of mean velocity profile parameters b(x), h(x) and U_c.

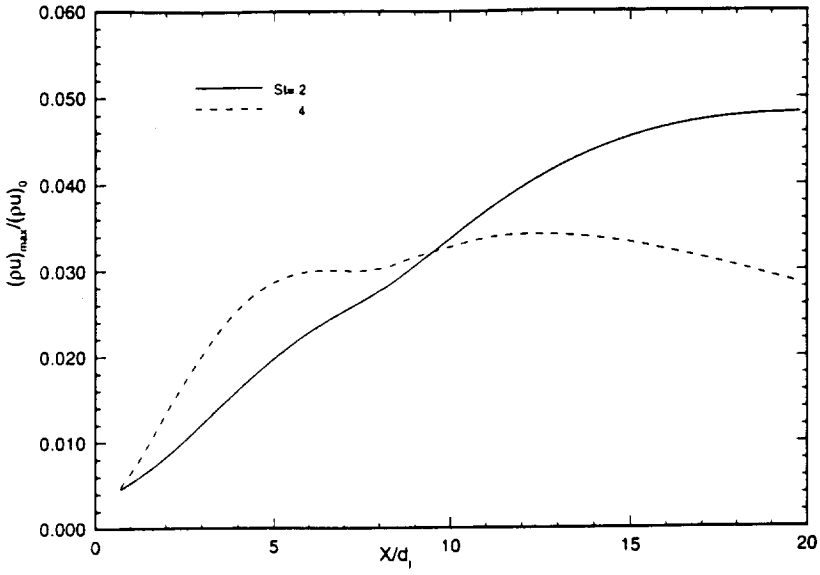

Figure 5. Axial distribution of mass velocity fluctuations in the shear layer for St=.2 and .4 and m=1.

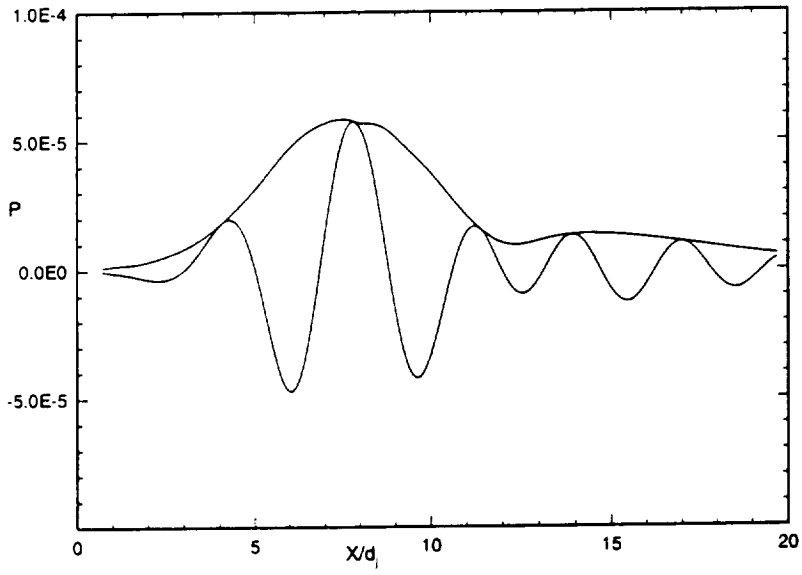

Figure 6. Pressure distribution at r/d_j=3 for St=.2 and m=1.

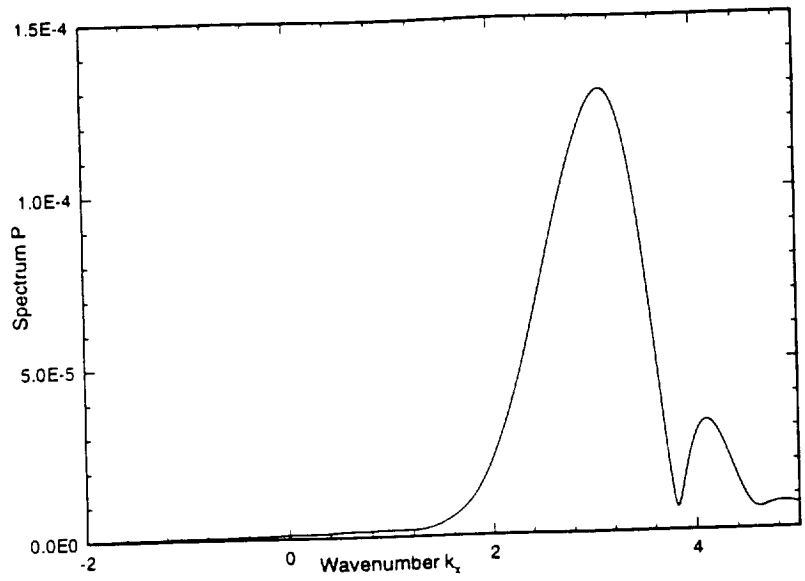

Figure 9. Spectral distribution of pressure $p_0(k_x)$ for St=.4 and m=1.

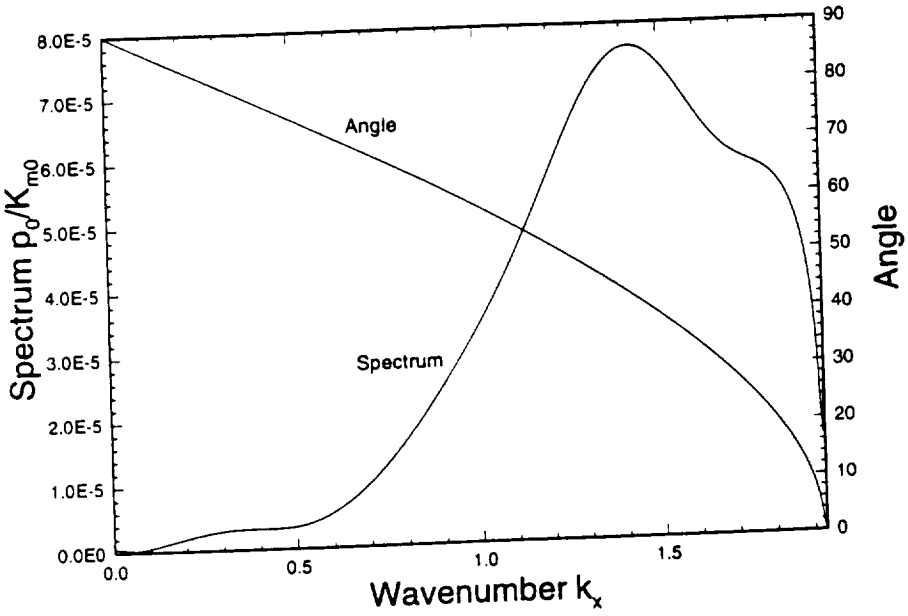

Figure 10. Distribution of $p_0(k_x)/K_{m0}(k_x)$ and the sound radiation angle given by eq.(23) for St=.2 and m=1.

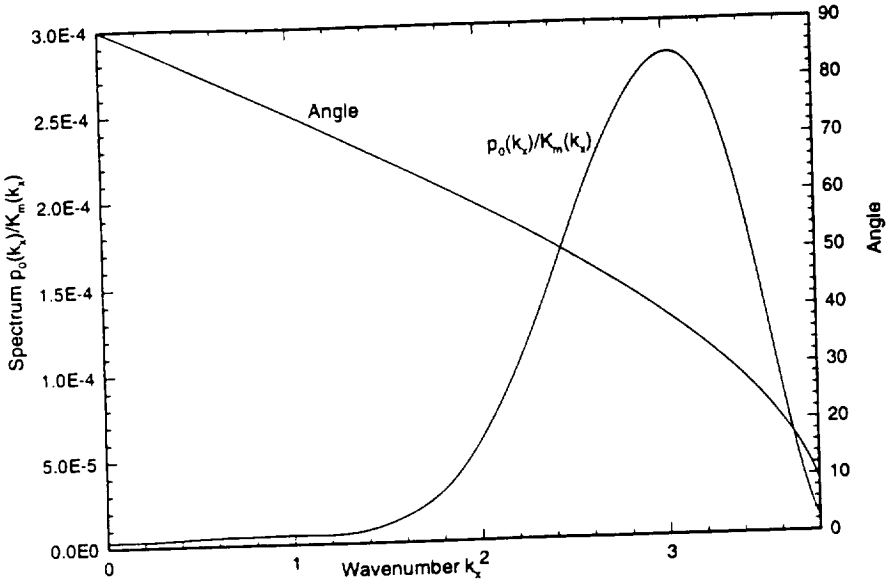

Figure 11. Distribution of $p_0(k_x)/K_{m0}(k_x)$ and the sound radiation angle given by eq.(23) for St=.4 and m=1.

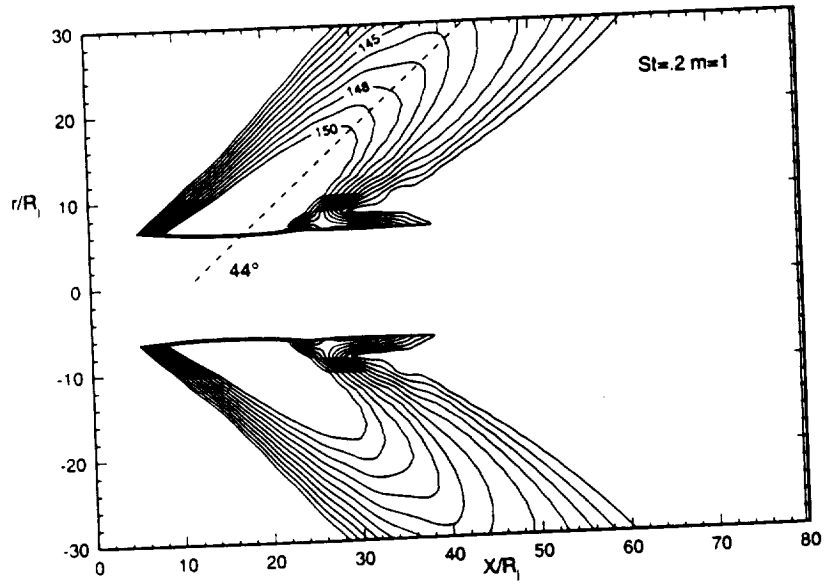

Figure 12. Sound pressure level contours computed from the wave equation for St=.2 and m=1.

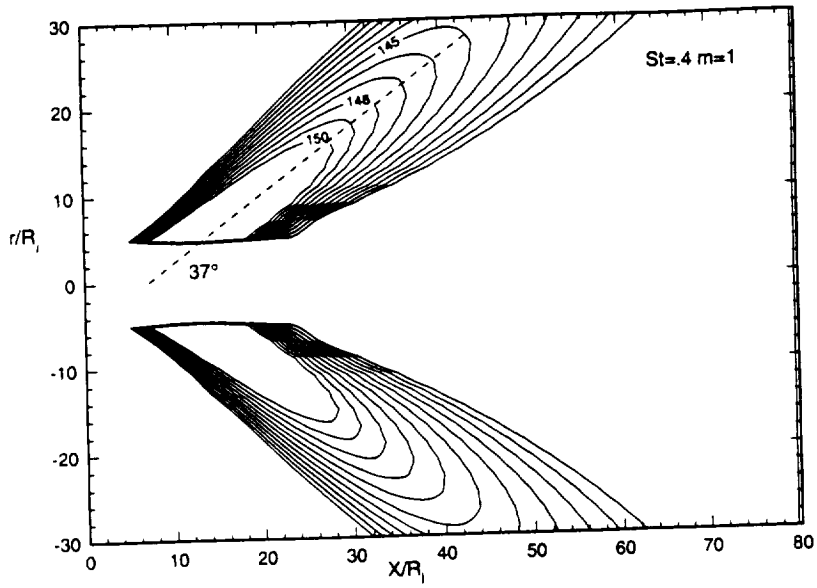

Figure 13. Sound pressure level contours computed from the wave equation for St=.4 and m=1.

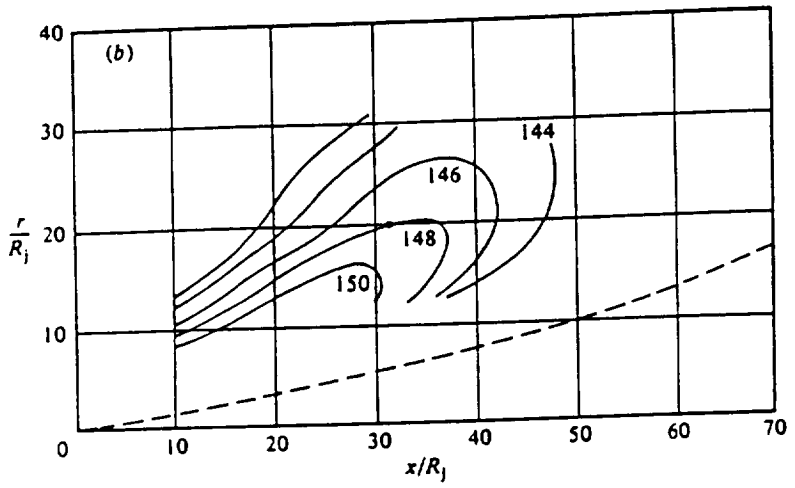

Figure 14. Sound pressure level contours measured by Troutt and McLaughlin (1982) for St=.2 and m=1.

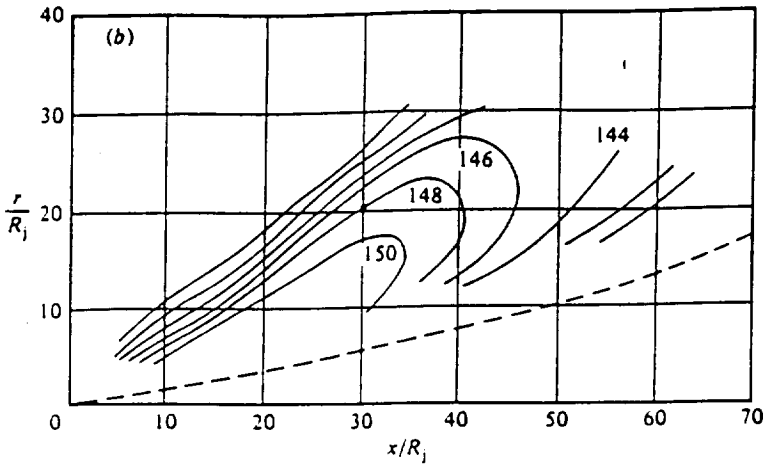

Figure 15. Sound pressure level contours measured by Troutt and McLaughlin (1982) for St=.4 and m=1.

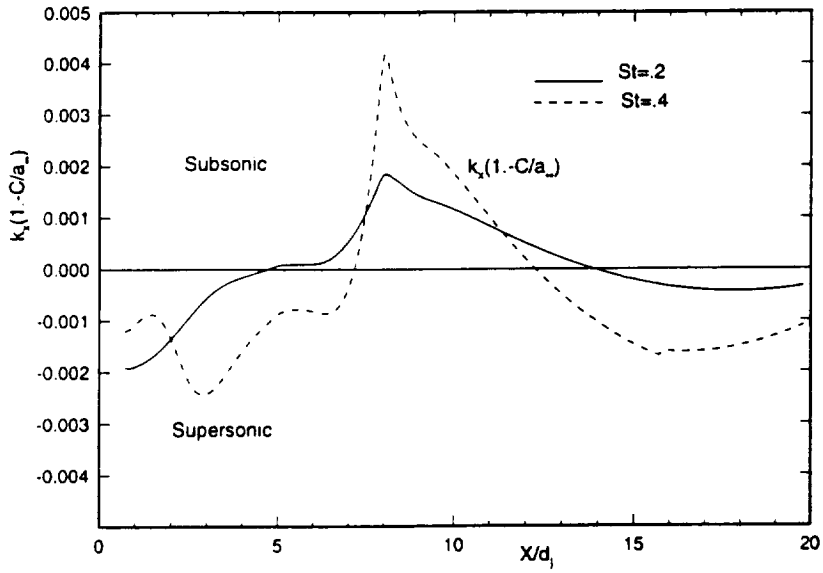

Figure 16. Axial distribution of the quantity (k_x-ωM) obtained from PSE for St=.2 and .4.

Jet stability and Noise Prediction Using Direct Numerical Simulation

Contents

1. Introduction
2. Governing equations
3. Numerical schemes
4. Boundary conditions
5. Noise calculations
    a) Mathematical formulations
    b) Numerical discretization
6. Results

References

1. Introduction:

The development of high speed civil transport plane requires reducing the jet exhaust noise. The computations of the jet noise radiated from the mixing layer may be divided into two parts. The first part is the evaluation of the near-field source and the second part is the computations of noise in the far field. In this work, we concentrate on obtaining the sound source using the direct numerical simulation of the full unsteady Navier-stokes equations.

Experiments by Laurence (1996) have shown that the sound power emitted from the jet is greatest within 4 to 5 diameters downstream and then decays through a transition region. This region is characterized by large vortical structures and is not fully turbulent (Soh 1994) which gives the motivation that we solve the unsteady flow equations using the direct numerical simulation (DNS) to provide the sound source for an acoustic computation of the far-field noise. Due to the limitations of the computational facilities available at the present time, the linearized Euler equations or the linearized wave equation is used to calculate the noise in the far field. The linearized Euler equations approach neglects both viscosity and nonlinear effects. The viscosity effects can be neglected since the free shear layer in the far field is essentially inviscid (Mankbadi 1992). The nonlinear flow effects and source generation are confined to the near field (Shih 1995) and sound propagation in the far-field can be modeled by linear instability waves. Tam and Morris (1980) calculated the noise in the far-field using the linear instability waves.

In order to evaluate the sound source using DNS, the simulation must be performed using numerical techniques with minimum distortion and diffusive characteristics. The numerical errors get worth for high Reynolds number flow simulations. Typically, free shear layer flows of interest have very high Reynolds numbers. Therefore, higher order accurate numerical schemes with minimum dissipation and dispersion errors are needed.

Part of this study is dedicated to the investigation of the accuracy of different numerical schemes.

The treatment of the boundaries is very important in getting an accurate solution of the Navier-stokes equations. Various computational techniques have been developed in the past to minimize the reflections of the out-going waves. Some of these techniques are based on the characteristics of the equations such as Thompson (1987) and Giles (1990). Other methods are based on the far-field asymptotic solution (Bayliss 1980, Enquist 1979, Hagstrom 1988, Tam 1993 and Tam 1995). In addition, a buffer zone technique has been developed in which the mean flow is altered gradually to be supersonic in a buffer region adjacent to the artificial boundaries (Givoli 1991, Street 1989 and Ta'asan 1995). A different approach has been proposed by Hu (1996) to damp the disturbance exponentially in a short layer called perfectly matching layer. We devoted part of this work to investigate different types of boundary conditions which will give minimum wave reflections near the boundaries.

In order to evaluate the jet stability and its radiated sound, the jet mean flow has to be computed. We used the boundary layer equations to solve for the jet mean flow. The equations are solved using two-point compact finite difference scheme. In addition, the linear stability theory is used to calculate the most unstable frequency for the jet and its eigenfunctions which will be used to excite the jet inflow boundary in DNS code. linearized Navier-stokes equations are used for the linear stability analysis.

It is widely believed that the large vortical structure and the vortex pairings are responsible for jet noise radiation (Colonius and et al. 1997 and Mitchel 1995), we investigated the sound generated by vortex roll-up and pairings by forcing the inflow with the most unstable frequency f and its subharmonics f/2 and f/4.

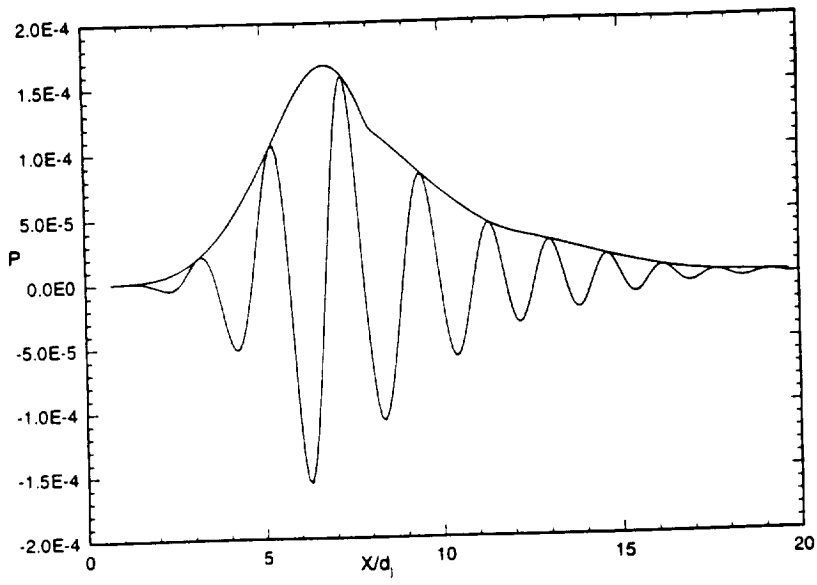

Figure 7. Pressure distribution at $r/d_j=3$ for St=.4 and m=1.

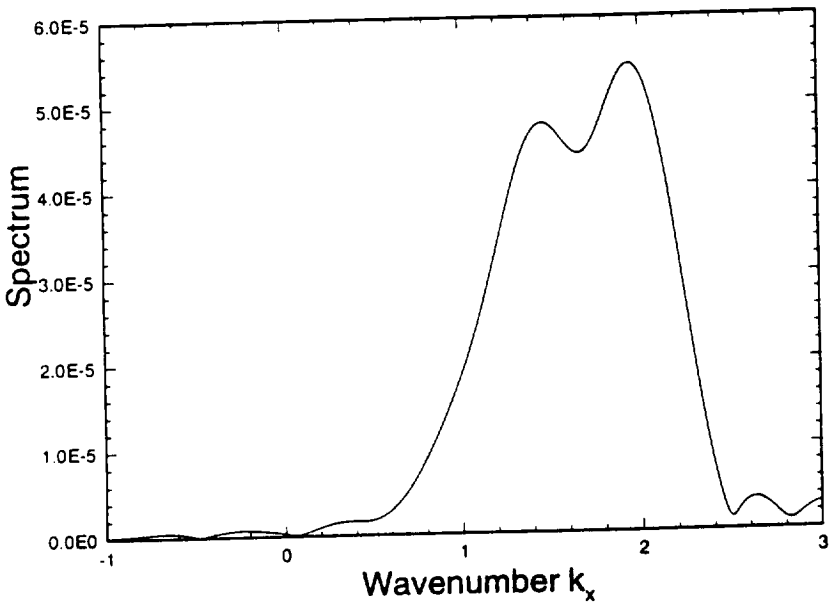

Figure 8. Spectral distribution of pressure $p_0(k_x)$ for St=.2 and m=1.

1. Governing Equations:

Navier-Stokes equations will be used to evaluate the near field source of jet noise and to compute the linear and nonlinear instability waves of the mixing layer. The equations are written in conservative form, cylindrical coordinates and for 3-d axisymmetric jet. The jet radius, exit velocity, temperature and density (r_j , u_j , T_j , ρ_j) are used to normalize the equations.

$$\frac{\partial Q}{\partial t}+\frac{\partial F}{\partial x}+\frac{1}{r}\frac{\partial rG}{\partial r}+\frac{1}{r}\frac{\partial H}{\partial \theta}=S \qquad (2.1)$$

$$Q=\begin{bmatrix}\rho\\ \rho u\\ \rho v\\ \rho w\\ \rho E\end{bmatrix}$$

$$F=\begin{bmatrix}\rho u\\ p+\rho u^2-\sigma_{xx}\\ \rho u v-\sigma_{xr}\\ \rho u w-\sigma_{x\theta}\\ (\rho \mathrm{E}+\mathrm{p})u-u\sigma_{xx}-v\sigma_{xr}-w\sigma_{x\theta}-k\frac{\partial T}{\partial x}\end{bmatrix}$$

$$G=\begin{bmatrix}\rho v\\ \rho u v-\sigma_{xr}\\ p+\rho v^2-\sigma_{rr}\\ \rho v w-\sigma_{r\theta}\\ (\rho \mathrm{E}+\mathrm{p})v-u\sigma_{xr}-v\sigma_{rr}-w\sigma_{r\theta}-k\frac{\partial T}{\partial r}\end{bmatrix}$$

$$H=\begin{bmatrix} \rho w \\ \rho u w-\sigma_{x\theta} \\ \rho v w-\sigma_{r\theta} \\ p+\rho w^2-\sigma_{\theta\theta} \\ (\rho E+p)w-u\sigma_{x\theta}-v\sigma_{r\theta}-w\sigma_{\theta\theta}-\dfrac{k}{r}\dfrac{\partial T}{\partial\theta} \end{bmatrix} \qquad S=\frac{1}{r}\begin{bmatrix} 0 \\ 0 \\ p+\rho w^2-\sigma_{\theta\theta} \\ -\rho v w+\sigma_{r\theta} \\ 0 \end{bmatrix}$$

$$p=(\gamma-1)\rho\left[E-\frac{1}{2}(u^2+v^2+w^2)\right]$$

$$T=\frac{p}{\gamma M_j^2 \rho}$$

Here Q is the unknown vector, F, G, and H are the fluxes in x, r, θ directions, respectively; S is the source term. The shear stresses are calculated as follows:

$$\sigma_{xx}=\frac{2\mu}{3\mathrm{Re}}(2\frac{\partial u}{\partial x}-\frac{v}{r}-\frac{\partial v}{\partial r}-\frac{1}{r}\frac{\partial w}{\partial 6})$$

$$\sigma_{\theta\theta}=\frac{2\mu}{3\mathrm{Re}}(\frac{2}{r}\frac{\partial w}{\partial 6}+\frac{2v}{r}-\frac{\partial u}{\partial x}-\frac{\partial v}{\partial r})$$

$$\sigma_{rr}=\frac{2\mu}{3\mathrm{Re}}(2\frac{\partial v}{\partial r}-\frac{v}{r}-\frac{\partial u}{\partial x}-\frac{1}{r}\frac{\partial w}{\partial 6})$$

$$\sigma_{xr}=\frac{\mu}{\mathrm{Re}}(\frac{\partial u}{\partial r}+\frac{\partial v}{\partial x})$$

$$\sigma_{x\theta}=\frac{\mu}{\mathrm{Re}}(\frac{1}{r}\frac{\partial u}{\partial 6}+\frac{\partial w}{\partial x})$$

$$\sigma_{r\theta}=\frac{\mu}{\mathrm{Re}}(\frac{1}{r}\frac{\partial v}{\partial 6}+\frac{\partial w}{\partial r}-\frac{w}{r})$$

and $\mathrm{Re}=\dfrac{\rho_j \mathrm{u}_j r_j}{\mu_j}$, $M_j=\dfrac{u_j}{\sqrt{\gamma R T_j}}$

The viscosity is calculated using Sutherland's law

$\mu=T^{3/2}\dfrac{T_j+110.4}{T+110.4}$ and the thermal conductivity is calculated from $k=\dfrac{\mu}{(\gamma-1)M_j^2\,\mathrm{Pr}\;\mathrm{Re}}$

2. Numerical Schemes:

MacCormack type schemes with operator splitting and high order accuracy developed by Hixon (1997), up to sixth order accurate in space and fourth order accurate in time, will be used in this simulation. The operators are applied in the following symmetric way:

$$Q^{n+2} = L_{2x} L_{2r} L_{2\theta} L_{1\theta} L_{1r} L_{1x} Q^n$$

Where L_x, L_r and L_θ, are one-dimensional operators in x, r and θ directions that are applied to these one-dimensional equations

$$Q_t = - F_x$$

$$Q_t = - G_r + S$$

$$Q_t = - H_\theta$$

The operators will be alternated with symmetrical variants such that the scheme will maintain the accuracy. Let L_1 be the operator with forward finite difference in the first step, then L_2 is the operator with backward finite difference in the first step.

Using Rung-Kutta, the equations are integrated in time as follows:

$$Q_t = -\frac{d}{dx}[F(Q)]$$

$$h_1 = -\Delta t \frac{d}{dx}^{f} [F(Q^n)]$$

$$h_2 = -\Delta t \frac{d}{dx}^{b} [F(Q^n + \alpha_2 h_1)]$$

$$h_3 = -\Delta t \frac{d}{dx}^{f} [F(Q^n + \alpha_3 h_2)]$$

$$h_4 = -\Delta t \frac{d}{dx}^{b} [F(Q^n + \alpha_4 h_3)]$$

$$h_5 = -\Delta t \frac{d}{dx}^{f} [F(Q^n + \alpha_5 h_4)]$$

$$h_6 = -\Delta t \frac{d}{dx}^{b} [F(Q^n + \alpha_6 h_5)]$$

$$Q^{n+1} = Q^n + \beta_1 h_1 + \beta_2 h_2 + \beta_3 h_3 + \beta_4 h_4 + \beta_5 h_5 + \beta_6 h_6$$

Accuracy	α_2	α_3	α_4	α_5	α_6	β_1	β_2	β_3	β_4	β_5	β_6
Second order	1	0	0	0	0	1/2	0	0	0	0	0
Fourth order	1/2	1/2	1	0	0	1/6	1/3	1/3	1/6	0	0
Multi-step (4-6) First step	1/2	1/2	1	0	0	1/6	1/3	1/3	1/6	0	0
Second step	.3533	.9996	.1522	.5342	.6039	.0468	.1373	.1710	.1976	.2823	.1651

Space discretization:

MacCormack schemes with higher order accuracy up to sixth order and minimum dispersion error are used. The forward and backward discretization for the fluxes are written in this form.

$$\left(\frac{dF}{dx}\right)^f = a_{-1}F_{i-1} + a_0F_i + a_1F_{i+1} + a_2F_{i+2} + a_3F_{i+3}$$

$$\left(\frac{dF}{dx}\right)^b = a_{-1}F_{i+1} + a_0F_i + a_1F_{i-1} + a_2F_{i-2} + a_3F_{i-3}$$

The accuracy of MacCormack schemes is increased to sixth order accurate by adding a point (a_3) to the discretization in the backward and forward directions. Also, the dispersion error is optimized for these schemes by adding another point (a_{-1}) such as 4/4, 6/4 and DRP/opt. Schemes as shown in the following table.

Scheme	a_{-1}	a_0	a_1	a_2	a_3
2/2	0	$\frac{-1}{\Delta x}$	$\frac{1}{\Delta x}$	0	0
4/2	0	$\frac{-7}{6\Delta x}$	$\frac{8}{6\Delta x}$	$\frac{-1}{6\Delta x}$	0
6/2	0	$\frac{-37}{30\Delta x}$	$\frac{45}{30\Delta x}$	$\frac{-9}{30\Delta x}$	$\frac{1}{30\Delta x}$
4/4	$\frac{-2}{6\Delta x}$	$\frac{-3}{6\Delta x}$	$\frac{6}{6\Delta x}$	$\frac{-1}{6\Delta x}$	0
6/4	$\frac{-9}{30\Delta x}$	$\frac{-19}{30\Delta x}$	$\frac{36}{30\Delta x}$	$\frac{-9}{30\Delta x}$	$\frac{1}{30\Delta x}$
DRP/opt	$\frac{-.30874}{\Delta x}$	$\frac{-.63254}{\Delta x}$	$\frac{1.2330}{\Delta x}$	$\frac{-.3334}{\Delta x}$	$\frac{.04168}{\Delta x}$

3. Boundary conditions:

4.1 Inflow B.CS:

For supersonic flow, all the flow variables are specified at the inflow boundary using

$$Q = Q_m + \varepsilon\, Q_{dist}$$

$$Q_{dist} = \sum_{k=0}^{2} \mathrm{Re}\, al[Q_k(r) e^{-i\omega t/2^k + i n\theta}]$$

where

Q_m is the mean flow variables,

$Q_k(r)$ are the eigenfunctions of the flow variables which are obtained from the linear stability code for the most unstable frequency ω and its subharmonics $\omega/2$ and $\omega/4$ and n is the azimuthal wave number. ε is the amplitude of the disturbance at the inflow boundary.

For subsonic flow, one flow variable is obtained from the interior points using the continuity equation and the rest of the flow variables are specified at the boundary as specified above.

$$\frac{\partial \rho}{\partial t} + \frac{\partial \rho u}{\partial x} + \frac{\partial \rho v}{\partial r} + \frac{1}{r}\frac{\partial \rho w}{\partial \theta} = -\frac{\rho v}{r}$$

The continuity equation may be written in the following characteristic form:

$$\frac{\partial \rho u}{\partial t} + [\lambda_2 + \frac{1}{2}(\lambda_1 + \lambda_5)]/c^2 + \frac{\partial \rho v}{\partial r} + \frac{1}{r}\frac{\partial \rho w}{\partial \theta} = -\frac{\rho v}{r}$$

where

$$\lambda_1 = (u - c)(\frac{\partial p}{\partial x} - \rho u \frac{\partial u}{\partial x})$$

$$\lambda_2 = u(c^2 \frac{\partial \rho}{\partial x} - \frac{\partial p}{\partial x})$$

$$\lambda_5 = (u + c)(\frac{\partial p}{\partial x} + \rho c \frac{\partial u}{\partial x})$$

For non-reflecting inflow boundary:

$\lambda_2=\lambda_5=0$ and λ_1 is calculated from the interior points.

4.2 Centerline Conditions:

Different techniques will be applied to overcome the singularity at the centerline for 3-D jet:

- Using the average values of the flow variables on the ring r=Δr. Prior to taking the average on the ring r=Δr, some conditions have to imposed on the ring r=0 based on the physics of the flow at the centerline. The first condition is obtained by noticing that the multivalued nature of the flowfield doesn't extend to pressure, temperature, density and axial component of the velocity. The radial and azimuthal components of velocity have multivalued at the centerline (Griffin et al. 1979). The second condition derives from the fact that the true velocity vector through any point can have only one direction in physical space, Since in our problem there is a symmetry plane (x, r plane) through which there can be no mass flow. If the velocity vector at a given point x on the centerline has the value U_{avg} , then the radial and azimuthal components (v , w) must be:

$$v(x,r,\theta) = U_{avg} \cos\theta$$
$$w(x,r,\theta) = -U_{avg} \sin\theta$$

To determine U_{avg} , one computes the average of the velocity vector U
On the ring using

$$U(x,r,\theta) = v(x,r,\theta)\cos\theta - w(x,r,\theta)\sin\theta$$

The average on the ring r=Δr is computed using this equation:

$$q_{i,j-1,l} = \frac{1}{k\max}\sum_{k=1}^{k\max} q_{i,j,k} \quad \text{, j=2, I=1,imax and l=1,kmax}$$

where $q = (\rho\ u\ U\ p\ T\ E)^t$

- Considering the centerline as an interior point with r=ε and using the same governing equations.
- Using Navier-stokes equations in Cartesian coordinates at the centerline only and using the following transformations to switch from Cartesian to polar coordinates and vice versa.

$$\begin{bmatrix} u_y \\ u_z \end{bmatrix} = \begin{bmatrix} \cos\theta & -\sin\theta \\ \sin\theta & \cos\theta \end{bmatrix} \begin{bmatrix} v \\ w \end{bmatrix} \quad , \quad \begin{bmatrix} v \\ w \end{bmatrix} = \begin{bmatrix} \cos\theta & \sin\theta \\ -\sin\theta & \cos\theta \end{bmatrix} \begin{bmatrix} u_y \\ u_z \end{bmatrix}$$

For 2-D jet, a new set of equations will be derived using L'Hospital rule. These equations will be applied with the following symmetric conditions:

$$\frac{\partial p}{\partial r} = \frac{\partial u}{\partial r} = \frac{\partial \rho}{\partial r} = 0$$
$$v = 0$$

4.3 Outflow and Radiation B.CS:

Different outflow and radiation B.CS will be investigated in this study.

i. Thompson's Characteristic B.CS:

The governing equations (1) could be written at x=L in the following characteristic form:

$$\frac{\partial Q}{\partial t} + d + \frac{1}{r}\frac{\partial rG}{\partial r} + \frac{1}{r}\frac{\partial H}{\partial 6} = C_x + S$$

where d is the amplitude of the characteristic waves and C is the shear stresses in x-direction.

$$d_1 = [\lambda_2 + (\lambda_1 + \lambda_5)/2]/C^2$$

$$d_2 = ud_1 + (\lambda_5 - \lambda_1)/2C$$

$$d_3 = vd_1 + \rho\,\lambda_3$$

$$d_4 = wd_1 + \rho\,\lambda_4$$

$$d_5 = \frac{1}{2}(u^2 + v^2 + w^2) * d_1 + \rho\,ud_2 + \rho\,vd_3 + \rho\,wd_4 + (\lambda_5 + \lambda_1)/[2(\gamma - 1)]$$

where

$$\lambda_1 = (u - c)\left(\frac{\partial p}{\partial x} - \rho\, c\frac{\partial u}{\partial x}\right) \qquad \lambda_2 = u\left(c^2\frac{\partial \rho}{\partial x} - \frac{\partial p}{\partial x}\right)$$

$$\lambda_3 = u\frac{\partial v}{\partial x} \qquad \lambda_4 = u\frac{\partial w}{\partial x}$$

$$\lambda_5 = (u + c)\left(\frac{\partial p}{\partial x} - \rho\, c\frac{\partial u}{\partial x}\right)$$

For nonreflecting outflow B.CS, all the incoming characteristics are set equal to zero and the outgoing characteristics are calculated from the interior points. Similar equations are obtained for the characteristics running in r-direction at r_{max}. In the

plane of intersection, both characteristic equations are applied. In the plane of symmetry at $\theta=0$ and $\theta=\pi$, symmetric B.CS are applied.

ii. Outflow Boundary [proposed by Rudy and Strikwerda (1980)]:

In these boundary conditions, a pressure correction term is added to the incoming waves in order to keep the pressure at the outflow close to the mean value. So, the incoming wave will be corrected as follows:

$$\lambda_5 = K(p - p_m)$$

where $K = \dfrac{\sigma(1 - M_{max}^2)C}{L}$.

M_{max} is the maximum Mach number in the flow field, C is the local speed of sound, L is a characteristic dimension of the domain, and σ is nonreflecting parameter ranges between zero and one.

iii. Buffer Domain B.CS:

The buffer - domain technique was proposed by Streett and Macaraeg (1989). The technique is based on gradually reducing the ellipticity of the Navier-Stokes equation. The sources of the ellipticity in the equations are the streamwise shear stresses and the pressure terms. To deal with these sources, the streamwise viscous terms and the pressure derivative in the streamwise direction are smoothly reduced to zero through multiplication by the following attenuation function:

$$S_j = \frac{1}{2}[1 + \tanh\{4(1 - 2\frac{j - N_b}{N_x - N_b})\}]$$

where N_b marks the beginning of the buffer domain and N_x marks the outflow boundary location.

iv. Perfectly Matching Layer:

In this technique, a region is added at the boundary as shown in figure (4.1) to damp the disturbance. In this region of the domain, exponential damping terms are added to the governing equation (2.1) of the form:

$$\frac{\partial Q1}{\partial t}+\frac{\partial (F-F_m)}{\partial x}+\sigma_x Q1=0$$

$$\frac{\partial Q2}{\partial t}+\frac{1}{r}\frac{\partial r(G-G_m)}{\partial r}+\sigma_y Q2=(S-S_m)$$

$$Q=Q1+Q2+Q_m$$

where $$\sigma_x=\sigma_{mx}\left(\frac{x-x^*}{L_b}\right)^{B_x}$$

where σ_{mx} is the maximum value of σ, L_b is the length of PML and x^* is the beginning of the Layer. Q_m, F_m, G_m and S_m denote the mean flow variables.

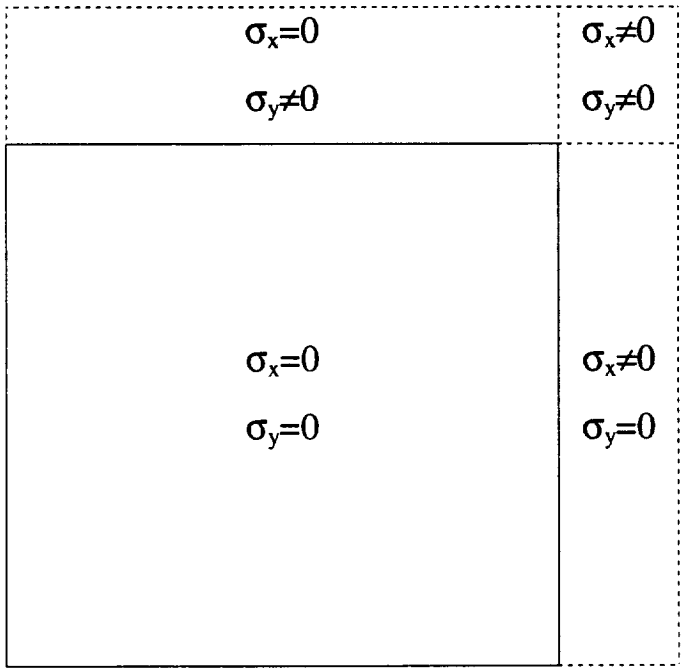

Figure (4.1): Computational Domain

5. Noise Calculations:

a. Mathematical formulations:

The jet noise and the pressure disturbance will be calculated in the far field using the linearized wave equation. The linearized Euler equations in cylindrical coordinates may be written as:

$$\frac{\partial u}{\partial t} = -\frac{1}{\rho_m}\frac{\partial p}{\partial x}$$
$$\frac{\partial v}{\partial t} = -\frac{1}{\rho_m}\frac{\partial p}{\partial r}$$
$$\frac{\partial w}{\partial t} = -\frac{1}{r\rho_m}\frac{\partial p}{\partial \theta} \qquad (5.1)$$
$$\frac{\partial p}{\partial t} + \frac{1}{M_o^2}\left(\frac{1}{r}\frac{\partial w}{\partial \theta} + \frac{v}{r} + \frac{\partial v}{\partial r} + \frac{\partial u}{\partial x}\right) = 0$$

Eliminating the velocity components from the last equation, we obtain the wave equation

$$\frac{\partial^2 p}{\partial t^2} - \frac{1}{\rho_m M_o^2}\left(\frac{1}{r^2}\frac{\partial^2 p}{\partial \theta^2} + \frac{1}{r}\frac{\partial v}{\partial r} + \frac{\partial^2 p}{\partial r^2} + \frac{\partial^2 p}{\partial x^2}\right) = 0 \qquad (5.2)$$

where ρ_m is the free stream mean density

and $M_o = \frac{u_j}{\sqrt{\gamma R T_o}}$, T_o is the free stream temperature

The wave equation (5.2) is solved with boundary conditions at $r=r_o$ and at the far field. At $r=r_o$ the pressure is known as function of time, azimuthal direction and axial position from the direct numerical simulation code and the pressure is applied as Dirichlet boundary condition.

$$p_o = p(x, r_o, \theta, t) \qquad (5.3)$$

At all other boundaries, the following radiation boundary condition derived by Tam (1980) is applied:

$$\frac{1}{C_o}\frac{\partial p}{\partial t} + \frac{\partial p}{\partial R} + \frac{p}{R} = 0 \qquad (5.4)$$

Where R is in the spherical coordinates and C_o is speed of sound in the far field.

$$R = \sqrt{x^2 + r^2}$$

Then equation (5.4) may be written in cylindrical coordinates as follows:

$$\frac{1}{C_o}\frac{\partial p}{\partial t} + \frac{x}{R}\frac{\partial p}{\partial x} + \frac{r}{R}\frac{\partial p}{\partial r} + \frac{p}{R} = 0 \qquad (5.5)$$

For two-dimensional axisymmetric jet, the inhomogenous term is divided by 2R rather than R (see two- and three-dimensional conditions by Roe 1989).

b. Numerical discretization:

The wave equation (5.2) is solved along with the boundary conditions (5.3) and (5.5) using six order compact finite difference Pade scheme and fourth order Runge Kutta is used to integrate the derivatives in time.

6. Results:

The results are presented here for two-dimensional subsonic and supersonic axisymmetric jet with high and low Reynolds numbers. Due to the limitations of the computational facilities, three-dimensional jet simulation is under development. The simulation is done for high subsonic jets at Mach numbers 0.8 and 0.85 while the supersonic jet results is presented for Mach number equal 2.5.

Figures (1) through (3) represent the variation of the mean flow axial velocity, radial velocity and temperature obtained from solving boundary layer equations for subsonic jet M_j=0.85 and Re=10^5. The mean flow parameters are slowly varying with axial direction due to the high Reynolds number used in the simulation. The most unstable frequency and its subharmonics are obtained from the linear stability analysis for this mean flow as shown in figure (4). The disturbance growth rate is decreasing with axial direction due to the mean flow variations. The most unstable frequency calculated for this flow is around 1.5 which gives Strauhal number of 0.477 ($st=f\, d_j /U_j$).

A comparison between different McCormack type numerical schemes is done to decide which scheme is suitable for the noise prediction. Figure (5.a) represent a comparison between the linear stability theory , 4/2 and DRP/optimized schemes for too many points per wave length. The two schemes give good results for 17 number of points per wave length. As the amplitude of the disturbance becomes large, the results do not agree with the linear stability because the linear stability theory is no longer valid. By decreasing the number of points per wave length, some of these schemes is not performing well as shown in figure (5.b). For 9 points per wave length, the dispersion and dissipation errors are significant for the 4/2 scheme. Other schemes like 6/2, 6/4 and DRR/opt. still have good accuracy.

Comparison between different outflow boundary conditions is introduced in figures (6) and (7). The reference solution is the long domain results where the computational domain is chosen to be long enough (x/r_j=100) such that the disturbance becomes steady and periodic in the required domain (x/r_j=60) before the disturbance hits the outflow boundary. It is clear from figure (7) that the perfectly matching layer technique gives

minimum reflections at the boundary and the buffer domain gives some reflections but it has less reflections than the characteristic boundary conditions proposed by Rudy (1980).

The pressure disturbance contours are presented in fig. (8) for supersonic hot jet (M_j=2.5) with zero free stream velocity and temperature ratio equal 2.25. It is clear that the pressure disturbance propagates within a cone which means that the noise radiation from the instability waves is confined within a wedge while the noise radiation from subsonic jet has no specific pattern as clear from fig. (9). There is upstream influence of the pressure waves for subsonic jet and the jet radiates noise in every direction. The density and vorticity contours are shown in figures (10) and (11) where the shear layer roll-up and the vortex pairings are clear.

The sound radiation by vortex roll-up and pairings for low Reynolds number subsonic jet (Re=2500, M_j=0.8) is investigated in figures (12)-(14).
The jet is excited at the inflow by the most unstable frequency f and its subharmonics f/2 and f/4. The Fourier transform of the energy amplitude is plotted in figure (12). It is clear from this graph that the second subharmonic is dominant . The energy grows in the linear region and then saturate at about x/r_j=40 for the second subharmonic where the source of the noise is located. The amplitude of the disturbance starts to decay after the saturation where the jet becomes turbulent. The vorticity contours plotted in fig. (13) shows the vortex pairs where the amplitude of the second subharmonic becomes large. This means that the large vortical structures are responsible for the noise radiation.

Using the wave equation, the sound pressure levels in the far field are calculated as shown in figure (14). No directivity pattern is predicted for the subsonic jet and the maximum sound pressure level obtained for a disturbance of amplitude 0.001 at the inflow is 140.5 decibels.

References:

1. Balakumar, P., 1998 "Prediction of supersonic jet noise" *AIAA paper* 98-1057
2. Bayliss, A. and Turkel, E., 1980 "Radiation boundary conditions for wave-like equations" *Communications on Pure and Applied Mathematics*, Vol. 33, pp. 708-725.
3. Bayliss, A. and Turkel, E., 1982 "Far field boundary conditions for compressible flows" *Journal of Computational Physics*, Vol. 48, pp. 182-199.
4. Berenger, J-P, 1994 "A perfectly matched layer for the absorption of electromagnetic waves" *Journal of Computational Physics*, Vol. 114, pp. 185-200.
5. Bridges, J. and Hussain, F., 1992 "Direct evaluation of aeroacoustic theory in a jet" *Journal of Fluid Mechanics*, Vol. 240, pp. 469-501.
6. Colonius, T., Lele, S. K. and Moin, P., 1993 "Boundary conditions for direct computation of aerodynamic sound generation" *AIAA Journal*, Vol. 31, No. 9, pp. 1574-1582.
7. Colonius, T., Sanjiva, K.L., Parviz, M., 1997 "Sound generation in a mixing layer" *Journal of Fluid Mechanics*, 1997, vol.330, pp. 375-409.
8. Dong, T. Z., 1996 " A set of simple radiation boundary conditions for acoustic computations in non-uniform mean flows" *AIAA* 96-0274.
9. Enquist, B. and Majda, A. , 1979 " Radiation boundary conditions for acoustic and elastic wave calculations" *Communications on Pure and Applied Mathematics*, Vol. 32 (3), {pp. 708-725}.
10. Freund, J.B., Lele, S.K., and Moin, P., 1998 " Direct simulation of a Mach 1.92 jet and its sound field" *AIAA/CEAS* 98-2291
11. Giles, M.B., 1990 " Nonreflecting boundary conditions for Euler equation calculations" *AIAA Journal*, Vol. 28, No. 12, pp. 2050-2058.
12. Givoli, D., 1991 " Non-reflecting boundary conditions" " *Journal of Computational Physics*, Vol. 94, pp. 1-29, 1991.
13. Griffin, M .D., Jones, E. and Anderson, J. D., 1979 "A computational fluid dynamic technique valid at the centerline for non-axisymmetric problems in cylindrical coordinates" *Journal of Computational Physics*, Vol. 30, pp. 352-360,1979.
14. Hagstrom, T. and Hariharan, S. I., 1988 " Accurate boundary conditions for exterior problems in gas dynamics" *Math. Computation*, Vol.51, pp. 581-597, 1988.
15. Hayder, M. E. and Turkel, E., 1995 "Nonreflecting boundary conditions for jet flow computations" *AIAA Journal*, Vol. 33, No. 12, pp. 2264-2270.
16. Hayder, M. E., Hu, F.Q. and Hussaini, M.Y., 1997 "Towards perfectly absorbing boundary conditions for Euler equations" *ICASE report* No. 97-25.
17. Hayder, M.E., Turkel, E., and Mankbadi, R.R., 1993 " Numerical simulation of a high Mach number jet" *AIAA* 93-0653
18. Hixon, R. and Shih, S. H., 1995 "Effect of input disturbance on linearized Euler equation prediction of jet noise" *AIAA* 95-0752.
19. Hixon, R. and Turkel, E., 1998 "High-accuracy compact McCormack-type schemes for computational aeroacoustics" *AIAA* 98-0365.
20. Hixon, R., 1997 "On increasing the accuracy of McCormack schemes for aeroacoustic applications" *AIAA* 97-1586-CP.
21. Hixon, R., Shih, S. H. and Mankbadi, R. R., 1995 "Evaluation of boundary conditions for computational aeroacoustics" *AIAA Journal*, Vol. 33, No. 11, pp. 2006-2012.

22. Hu, F.Q., 1995 "On absorbing boundary conditions for linearized Euler equations by a perfectly matching layer" *ICASE Report* 95-70.
23. Joslin, R.D, Street, C.L., and Chang, C.L., 1992 " Validation of three-dimensional incompressible spatial direct numerical simulation code" *NASA technical paper* 3205.
24. Khorami, M.R., 1991 " Stability of a compressible swirling jet" *AIAA* 91-1770.
25. Laufer, J. and Yen, T-C., 1983 "Noise generation by a low-Mach-number jet" *Journal of Fluid Mechanics*, Vol. 134, pp.1-31.
26. Laurence, J. C., 1956 "Intensity scale and spectra of turbulence in mixing region of free subsonic jet" *NACA Rep.* No. 1292.
27. Mankabadi, R. R., 1990 "The self-noise from ordered structures in a low Mach number jet" *Journal of Applied Mechanics*, Vol. 57, pp. 241-246.
28. Mankbadi, R. R., 1992 "Dynamics and control of coherent structures in turbulent jets" *Appl. Mech. Review*, Vol. 45, pp. 219-248.
29. Mankbadi, R.R, Hayder, M.E, and Povinelli, L.A, 1994 " Structure of supersonic jet flow and its radiated sound" *AIAA Journal*, Vol. 32, No. 5, pp. 897-906.
30. Mitchel, B. E., Lele, S. K. and Moin, P., 1995 "Direct computation of the sound generated by vortex pairing in an axisymmetric jet" *AIAA* 95-0504.
31. Poinsot, T. J. and Lele, S. K., 1992 "Boundary conditions for direct simulations of compressible viscous flows" *Journal of Computational Physics*, Vol. 101, pp. 104-129.
32. Roe, P. L., 1989 "Remote Boundary conditions for unsteady multidimensional aerodynamic computations" *Computer and Fluids Journal*, Vol. 17, No. 1, pp.221-231, 1989.
33. Rudy, D. and Strikwerda, J. C., 1980 "Nonreflecting outflow boundary condition for subsonic Navier-stokes calculations" *Journal of Computational Physics*, Vol. 36, pp. 55-70.
34. Scott, J.N., 1993 "Accuracy consideration in the computational analysis of jet noise" *AIAA* 93-0146.
35. Shih, S. H. and Hixon, D. R., 1995 "A zonal approach for prediction of jet noise" *CEAS/AIAA*-95-144.
36. Shih, S. H., Hixon, R. and Mankbadi, R.R., 1995 "Three dimensional structure in a supersonic jet: behavior near centerline" *AIAA* 95-0508.
37. Shih, S.H., Hixon, D.R., 1996 " prediction of flow and acoustic fields of a supersonic jet" *AIAA* 96-0751
38. Soh, W. Y., 1994 "Unsteady jet flow computation towards noise prediction" *AIAA* 94-0138.
39. Street, C. L., Magaraeg, M. G., 1989 "Spectral multi-domain for large-scale fluid dynamics simulations" *Int. Journal Appl. Numer. Math.*, Vol. 6, pp. 123-139,1989.
40. Ta'asan, S. and Nark, D. M., 1995 "An absorbing buffer zone technique for acoustic wave propagation" *AIAA* 95-0164.
41. Tam, C. K.W. and Morris, P. J., 1980 "The radiation of sound by instability waves of a compressible plane turbulent shear layer" *Journal of Fluid Mechanics*, Vol. 98, pt.2, pp. 349-381.
42. Tam, C. K. W. and Dong, Z, 1995 "Radiation and outflow boundary conditions for direct computation of acoustic and flow disturbances in a nonuniform mean flow" *CEAS/AIAA* 95-007.

43. Tam, C. K. W. and Webb, J. C., 1993 "Dispersion relation preserving schemes for computational acoustics" *Journal of Computational Physics*, Vol. 107, pp. 262-281, 1993.
44. Tam, C. K.W. and Dong, Z. 1994 "Wall boundary conditions for high-order finite difference schemes in computational aeroacoustics" *AIAA* 94-0457.
45. Tam, C. K.W., 1995 "Computational aeroacoustics issues and methods" *AIAA* 95-0677.
46. Thompson, K. W., 1987 "Time-dependent boundary conditions for hyperbolic systems" *Journal of Computational Physics*, Vol. 68, pp. 1-24.
47. Trefethen, L.N., 1982 "Group velocity in finite difference schemes" *SIAM Review*, Vol. 24, No.2, April 1982.
48. Vichnevetsky, R., 1986 " Invariance theorems concerning reflections at numerical boundaries" *Journal of Computational Physics*, Vol. 63, pp. 268-282, 1986.
49. Viswanathan, K. and Sankar, L. N., 1995 "Toward the direct calculation of noise: Fluid/Acoustic coupled simulation" *AIAA Journal*, Vol. 33, No. 12, pp.2271-2279.

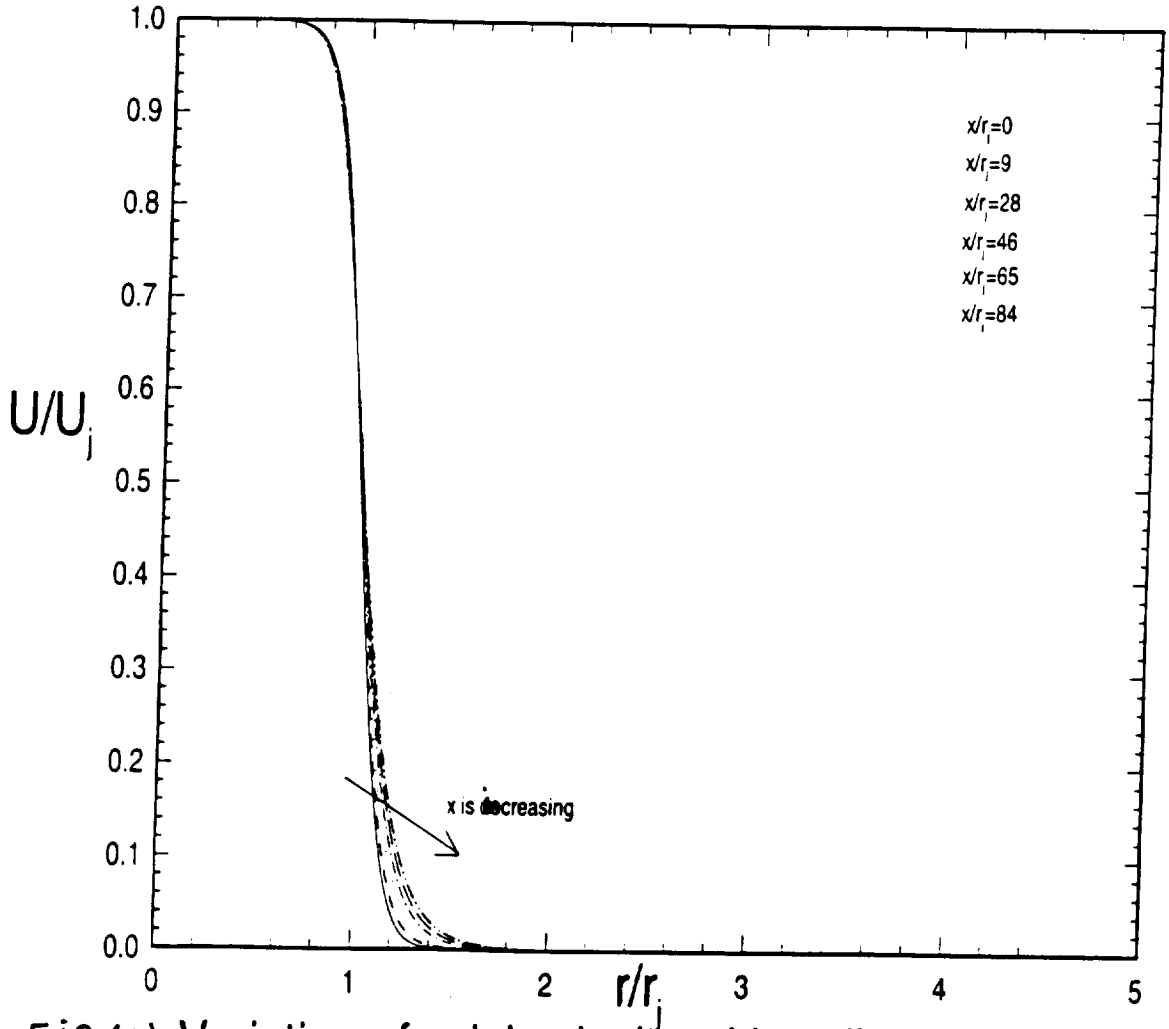

Fig (1) Variation of axial velocity with radial distance

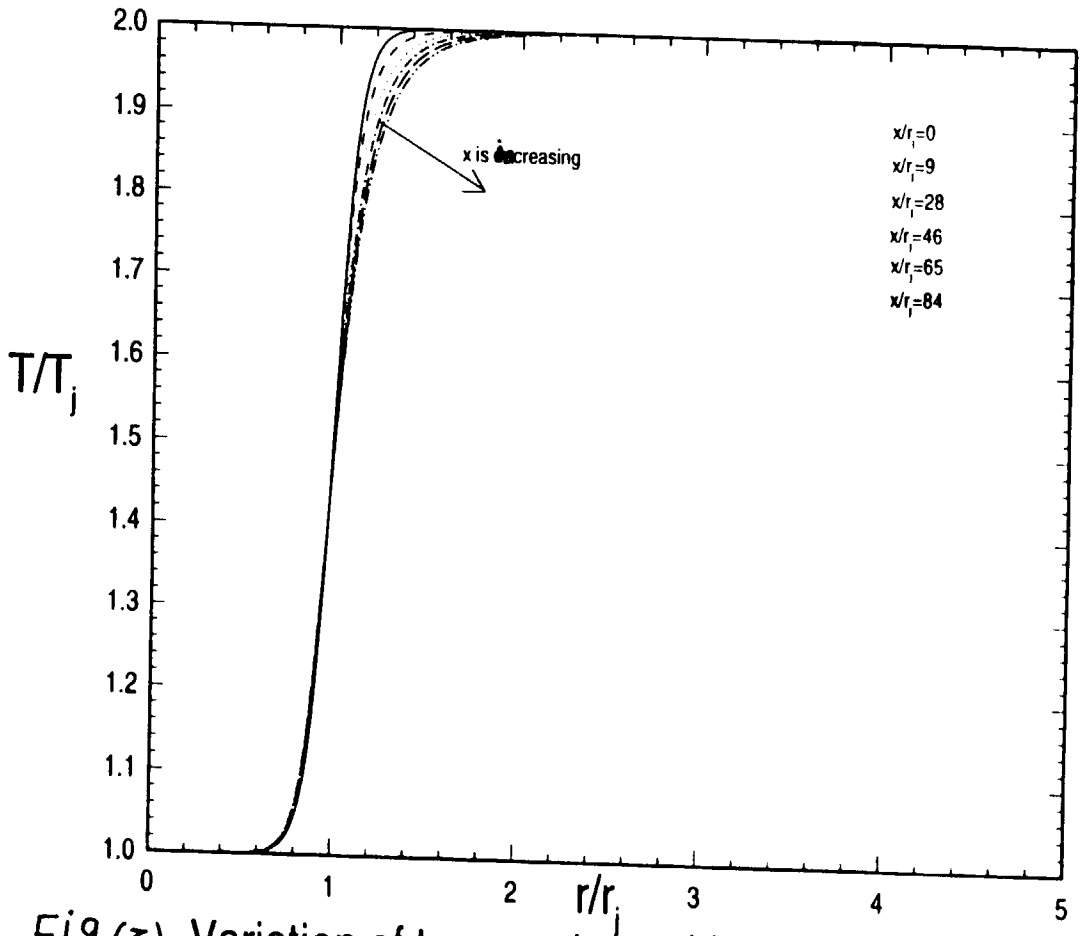

Fig (3) Variation of temperature with radial distance

Fig (4) *Growth rate versus frequency for subsonic jet*
$Re=10^5$ $M_j=0.85$ $U_o/U_j=0$

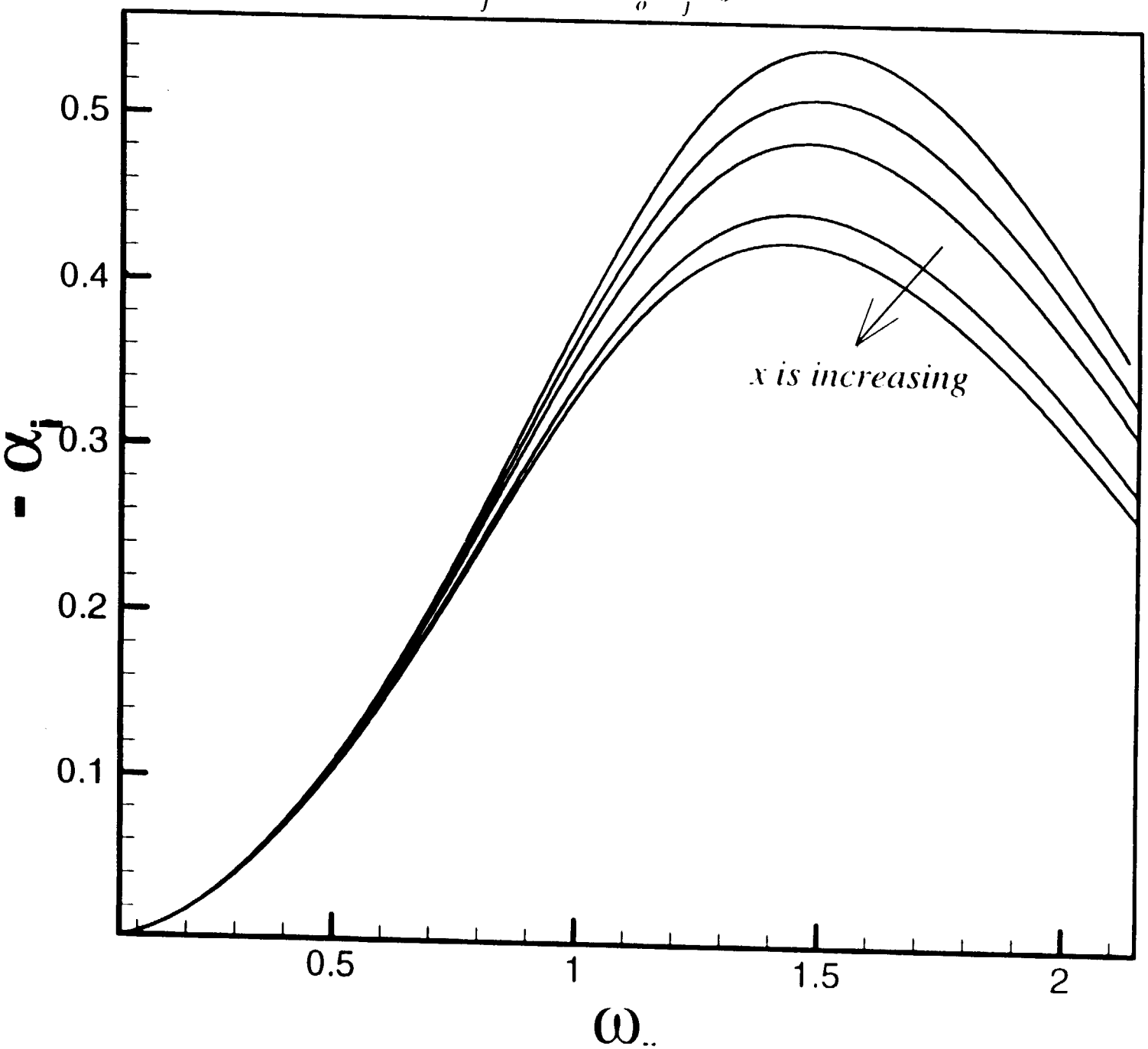

Fig (5) Comparison bet. LS, Drp, and 4/2 schemes

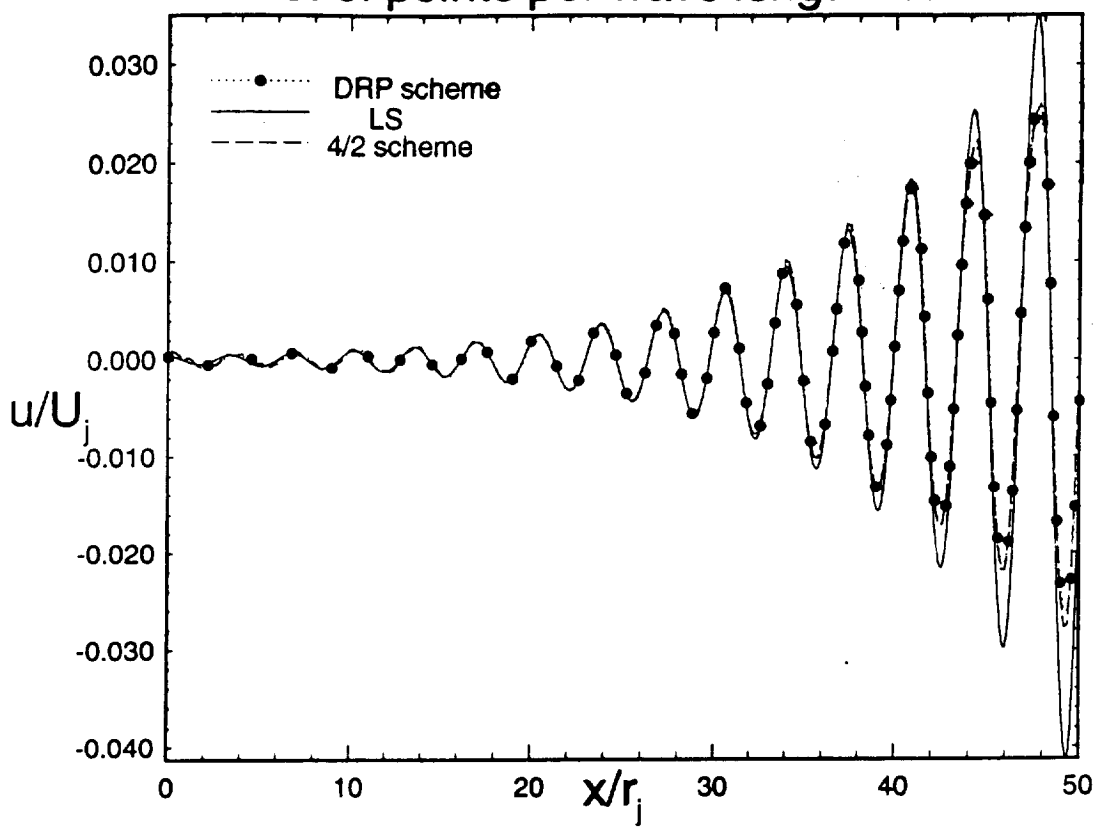

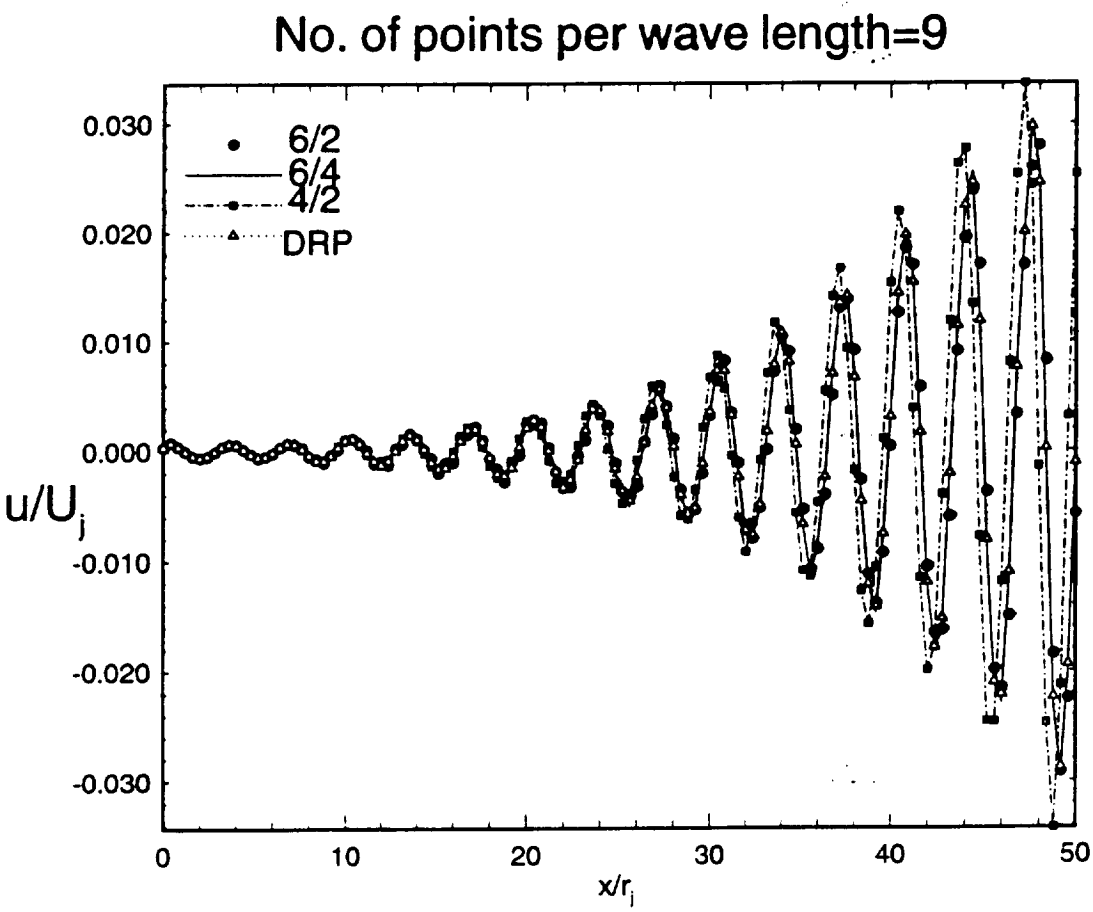

Fig(6) Subsonic Jet M_j=0.85, Re=10^5, U_0/U_j=0.2, St.=0.453

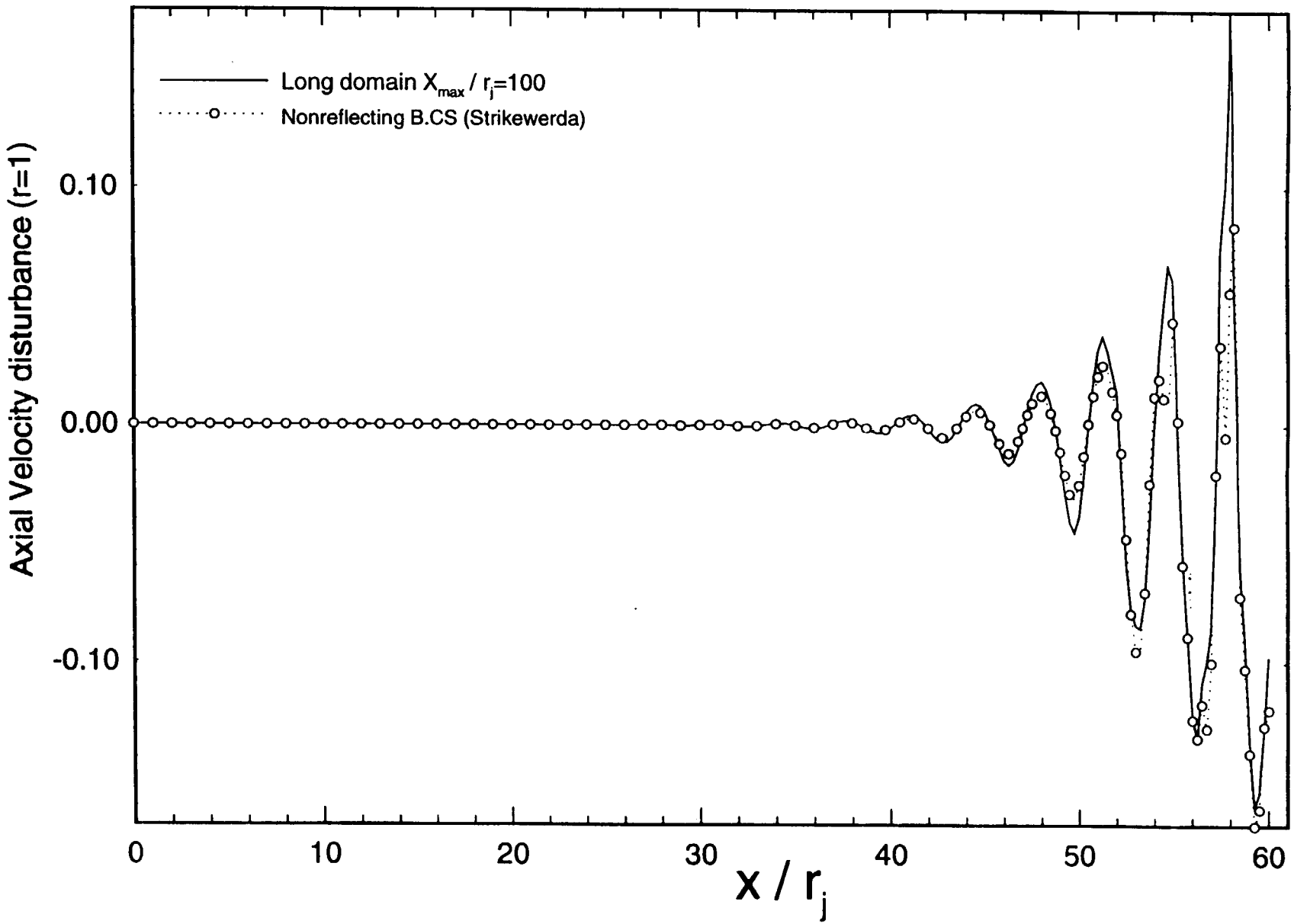

Fig(7) Subsonic Jet M_j=0.85, Re=10^5, U_0/U_j=0.2, St.=0.453

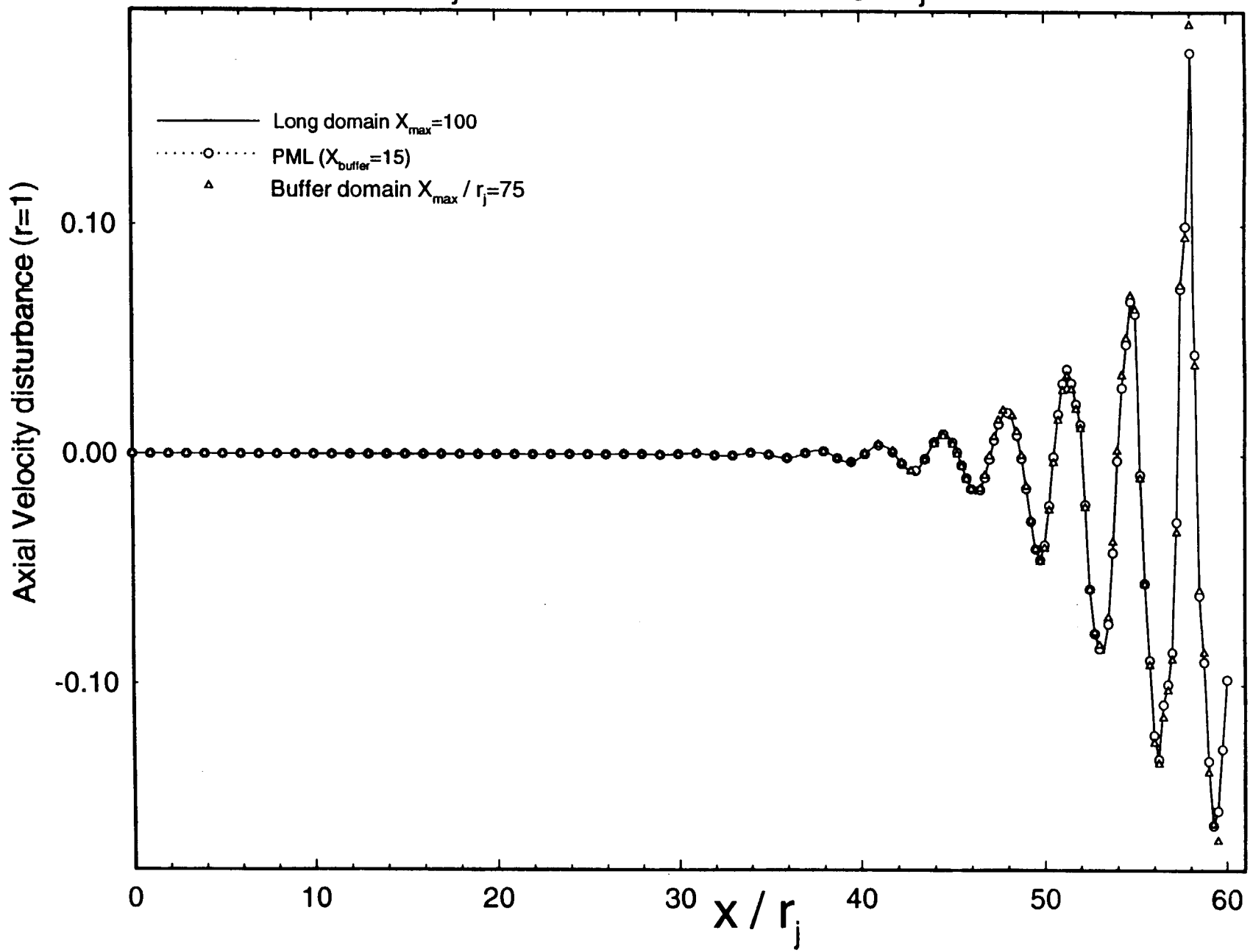

Fig (8) Pressure Disturbance Contours for supersonic Jet

M_j=2.5, Re=4350, St=0.382, U_o/U_j=0, T_o/T_j=2.25

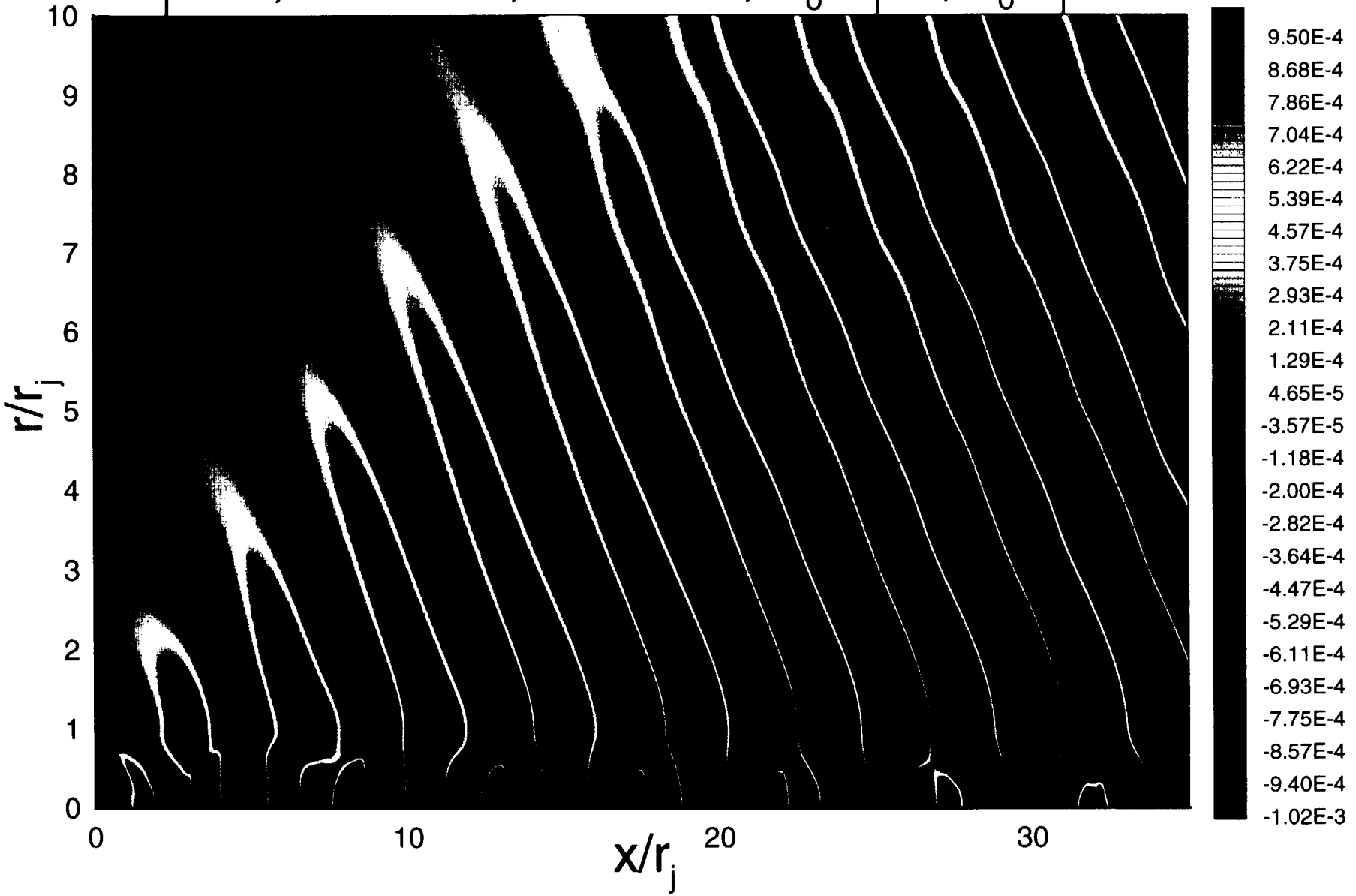

Fig(9) Pressure Disturbance Contours for High Subsonic Jet

M_j=0.85, Re=10^5, U_o/U_j=0, T_o/T_j=2.0

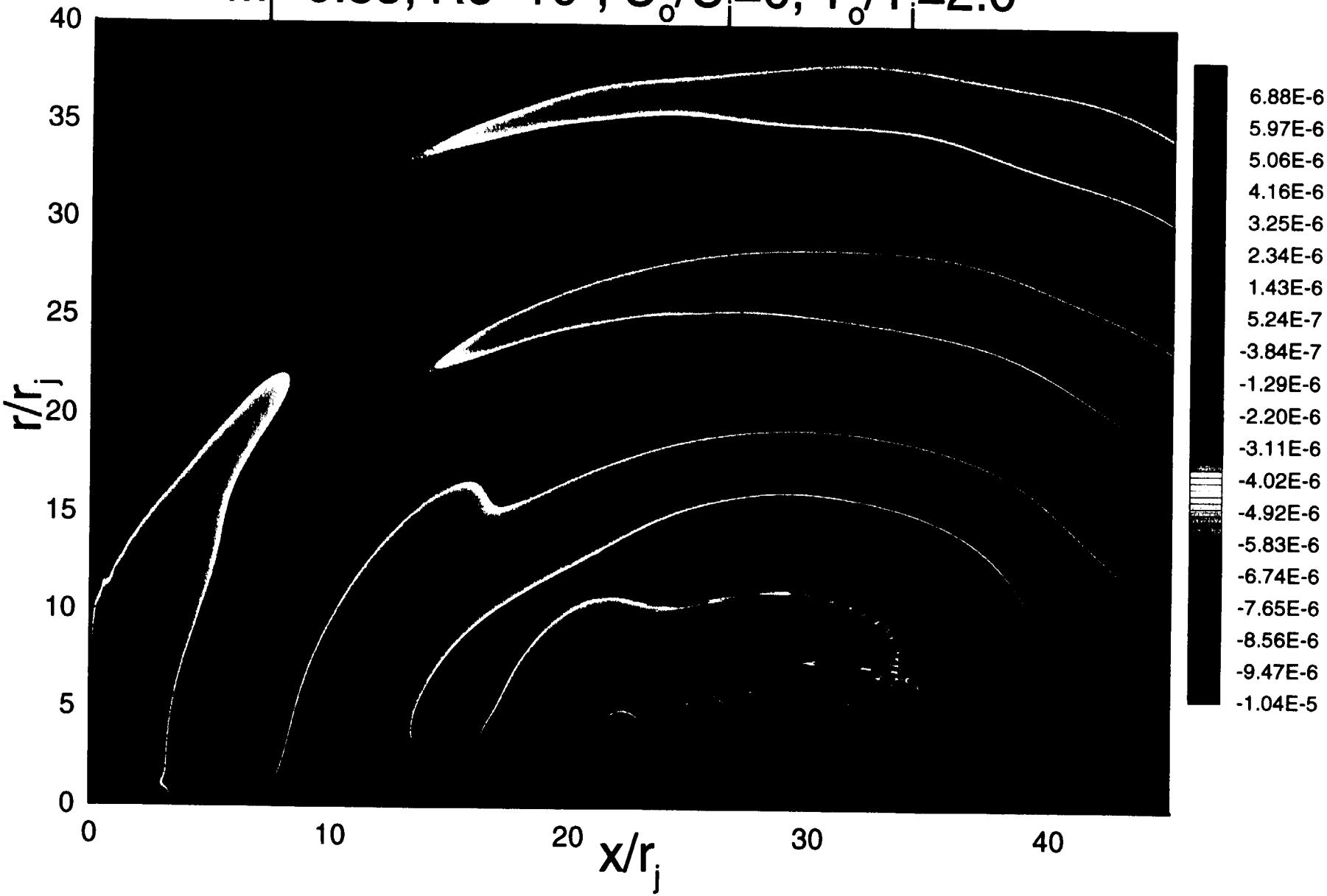

Fig (10) Density Contours for High Subsonic Jet
M_j=0.85, Re=10^5, U_o/U_j=0, T_o/T_j=2.0

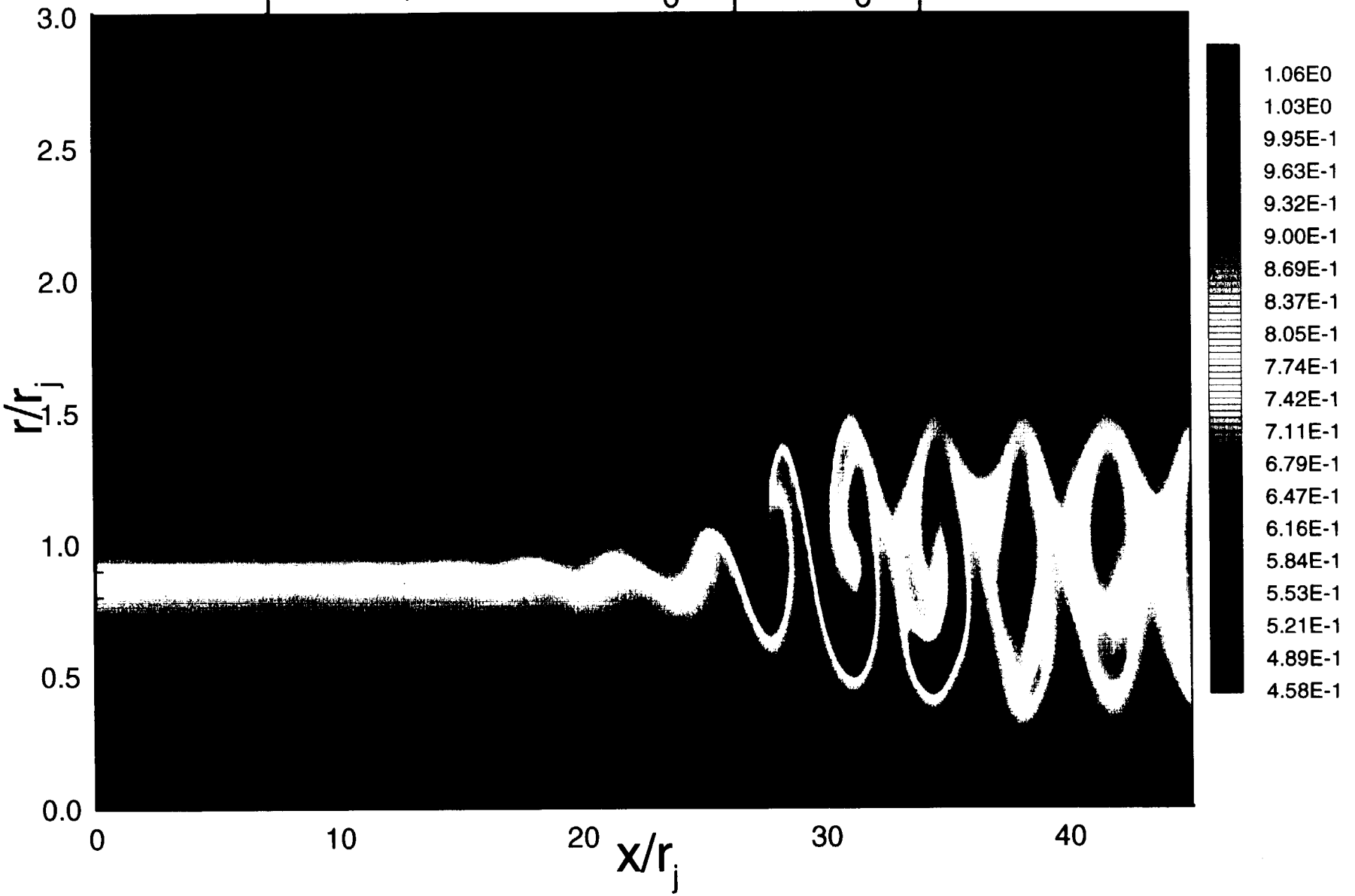

Fig(11) Vorticity Contours for High Subsonic Jet
M_j=0.85, Re=10^5, U_o/U_j=0, T_o/T_j=2.0

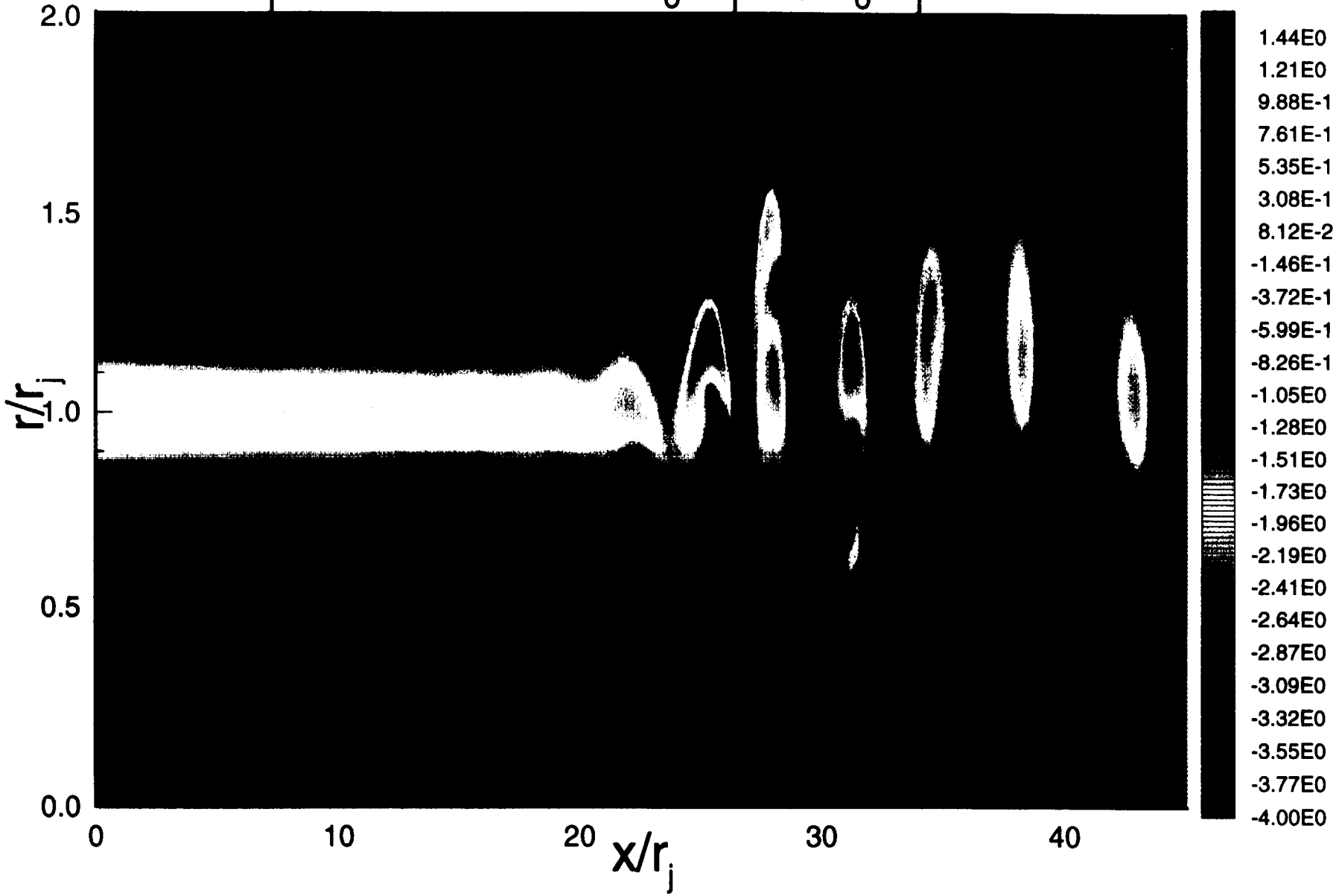

Fig. (12) *Frequency analysis for nonlinear subsonic Jet M_j=0.8*

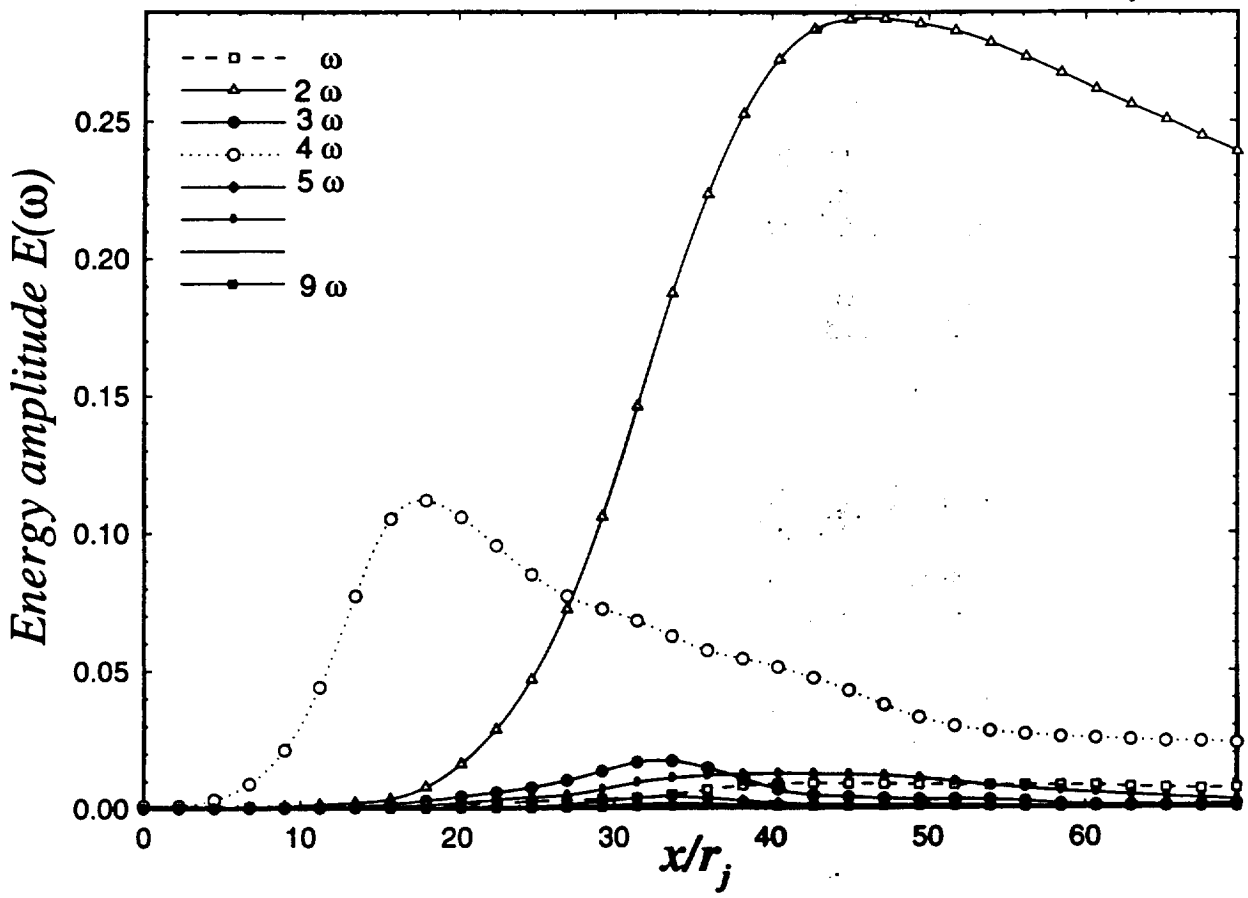

Fig(13) ***Vorticity contours for subsonic Jet***
M_j=0.8, Re=2500

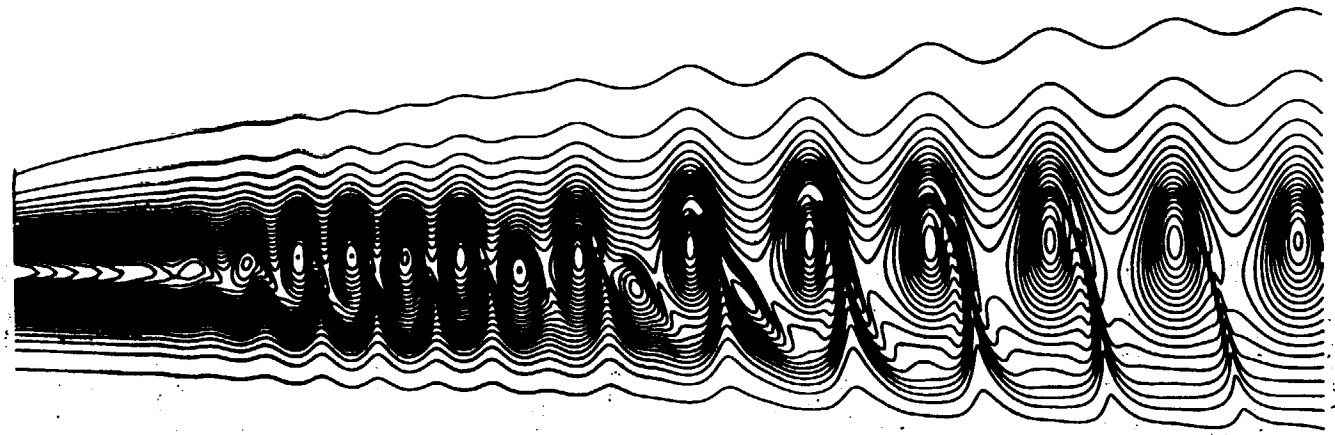

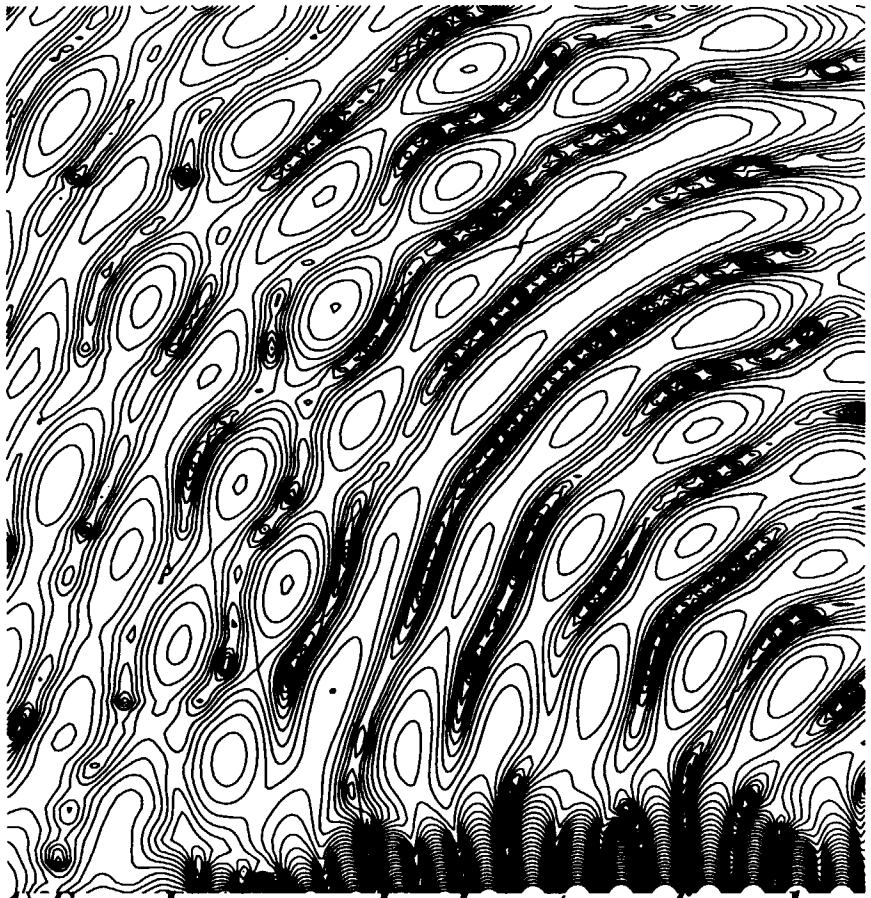

Fig. (14) Sound pressure level contours for subsonic jet $M_j = 0.8$, $Re = 2500$